

# Direct Relationship between Protein Expression and Progeny Yield of Herpes Simplex Virus 1 Unveils a Rate-limiting Step for Virus Production

Moeka Nobe<sup>1,†</sup>, Yuhei Maruzuru<sup>1,2,3,†</sup>, Kosuke Takeshima<sup>1,2,3</sup>, Fumio Maeda<sup>4</sup>, Hideo Kusano<sup>4,5</sup>, Raiki Yoshimura<sup>6</sup>, Takara Nishiyama<sup>6</sup>, Hyeongki Park<sup>6</sup>, Yoshitaka Kozaki<sup>6</sup>, Shingo Iwami<sup>6</sup>, Naoto Koyanagi<sup>1,2,3</sup>, Akihisa Kato<sup>1,2,3</sup>, Tohru Natsume<sup>4</sup>, Shungo Adachi<sup>4,5</sup>, and Yasushi Kawaguchi<sup>1,2,3,7\*</sup>

<sup>1</sup>Division of Molecular Virology, Department of Microbiology and Immunology, The Institute of Medical Science, The University of Tokyo, Tokyo, Japan

<sup>2</sup>Department of Infectious Disease Control, International Research Center for Infectious Diseases, The Institute of Medical Science, The University of Tokyo, Minato-ku, Tokyo 108-8639, Japan

<sup>3</sup>Research Center for Asian Infectious Diseases, The Institute of Medical Science, The University of Tokyo, Tokyo, Japan

<sup>4</sup>Molecular Profiling Research Center for Drug Discovery (molprof), National Institute of Advanced Industrial Science and Technology (AIST), Tokyo, 135-0064, Japan.

<sup>5</sup>Department of Proteomics, National Cancer Center Research institute, Tokyo, Japan

<sup>6</sup>Interdisciplinary Biology Laboratory (iBLab), Division of Biological Science, Graduate School of Science, Nagoya University, Nagoya 464-8602, Japan

<sup>7</sup>The University of Tokyo, Pandemic Preparedness, Infection and Advanced Research Center, Tokyo, Japan

**Short title: A Rate-limiting Step for HSV-1 Production**

\*Address correspondence to:

Dr. Yasushi Kawaguchi

Division of Molecular Virology

Department of Microbiology and Immunology

The Institute of Medical Science

The University of Tokyo

32 4-6-1 Shirokanedai, Minato-ku, Tokyo 108-8639, Japan

33 Phone: 81-3-6409-2070

34 Fax: 81-3-6409-2072

35 E-mail: [ykawagu@ims.u-tokyo.ac.jp](mailto:ykawagu@ims.u-tokyo.ac.jp)

36

37 †These authors contributed equally to this work.

38

## ABSTRACT

39 Although viral protein expression and progeny virus production were independently  
40 shown to be highly heterogenous in individual cells, their direct relationship, analyzed by  
41 considering their heterogeneities, has not been investigated to date. This study established  
42 a system to fractionate cells infected with a herpesvirus based on the levels of the global  
43 expression of viral late proteins, which are largely virion structural proteins, and to titrate  
44 virus yields in these fractions. This system demonstrated a direct relationship and  
45 indicated there was a threshold for the levels of viral late protein expression for progeny  
46 virus production and suggested that viral DNA cleavage/packaging was a rate-limiting  
47 step for progeny virus production. These findings, which were masked in previous studies  
48 performed at the entire population level, have uncovered a sophisticated viral strategy for  
49 efficient progeny virus production and shed new light on an effective target for the  
50 development of anti-viral drugs.

## INTRODUCTION

The state of viral gene expression has long been thought to be one of the critical determinants for virus progeny production<sup>1</sup>. Viral infection is usually studied at the entire population level by averaging the outcomes of infection from each of large numbers of individual cells. In these previous studies, a relationship between viral gene expression and virus progeny production has necessarily been investigated based on classical time course experiments in which levels of viral gene expression and progeny virus titers were compared at various times after infection. Such studies demonstrated that the levels of viral gene expression, including the expressions of viral mRNA and protein, correlated well with progeny virus yields<sup>2-6</sup>. However, accumulating evidence has indicated that viral infection at the single-cell or subpopulation level is highly heterogeneous, which has been masked in studies performed at the entire population level. Thus, it was reported that the progeny virus yield from individual cells spanned several orders of magnitude<sup>7-14</sup>. Classical fluorescence microscopy and recent advances in single-cell RNA-sequencing have enabled the investigation of the state of viral gene expression at the single-cell level, revealing high heterogeneity in individual cells and identifying new subpopulations of infected cells with similar viral gene expression profiles<sup>15-17</sup>. However, there is a lack of information on viral protein expression and virus progeny production in the same

individual cell or subpopulation. Therefore, the direct relationship between viral protein expression and progeny virus production, analyzed by considering their heterogeneities at single cell or subpopulation levels, remains to be elucidated. These observations raised a fundamental question as to whether the well-established correlation between viral protein expression and progeny virus production detected at the entire population level by classical time-course experiments<sup>4,6</sup> does reflect a direct relationship between them.

Herpes simplex virus 1 (HSV-1), an extensively studied DNA virus, is a ubiquitous human pathogen, causing a variety of diseases including encephalitis, keratitis, and mucocutaneous and skin diseases including herpes labialis, genital herpes and herpetic whitlow<sup>18</sup>. HSV-1 encodes more than 100 different proteins<sup>19-21</sup> and HSV-1 genes fall into three major classes: immediate-early (IE), early (E) and late (L), whose expressions are coordinately regulated and sequentially ordered in a cascade during lytic infection<sup>19</sup>. Although there are some exceptions, virion structural proteins are largely encoded by L genes<sup>19</sup>. Replication of the HSV-1 genome and packaging of the replicated viral genomes into nascent capsids occurs in the nucleus<sup>19</sup>. Nascent nucleocapsids are exported to the cytoplasm through the perinuclear space between the inner nuclear membrane and outer nuclear membrane by a nuclear pore-independent and sequential

86 envelopment/de-envelopment process <sup>19</sup>. In the cytoplasm, capsids acquire a final  
87 envelope by budding into cytoplasmic vesicles and become infectious <sup>19</sup>.

88 In this study, we constructed a reporter HSV-1 to monitor the global expression  
89 of viral L proteins by analyzing direct and quantitative relationship between L protein  
90 expression levels and virus progeny yields by sorting infected cells into subpopulations  
91 based on reporter gene expression levels and by determining virus titers in the  
92 subpopulations. The clarified relationship indicated a threshold in the levels of HSV-1 L  
93 protein expression for progeny virus production, suggesting viral DNA  
94 cleavage/packaging is a rate-limiting step for progeny virus production.

95

## RESULTS

### **Construction and characterization of a reporter HSV-1 to analyze viral L protein**

### **expression and virus progeny yields at the subpopulation level.**

We constructed a recombinant virus rICP47/vUs11 expressing IE protein ICP47 and L protein Us11 fused

to monomeric fluorescent proteins, TagRFP and VenusA206K (TagRFP-ICP47 and

Venus-Us11), respectively (Fig. 1A and B). The growth of rICP47/vUs11 was similar to

wild-type HSV-1(F) in HeLa cells at a multiplicity of infection (MOI) of 5 and reached a

plateau 24 h after infection (Fig. 1C). Flow cytometric analyses showed 92% of HeLa

cells inoculated with rICP47/vUs11 at an MOI of 5 were TagRFP positive 24 h after

inoculation, indicating that in these experimental settings, most HeLa cells were infected

with rICP47/vUs11 and HSV-1 gene expression was initiated in these infected cells (Fig.

1D and E). Frequencies of cells positive for Venus and TagRFP, or those positive for

TagRFP and negative for Venus, were 67% and 25%, respectively (Fig. 1E). Cells

positive for Venus and negative for TagRFP were barely detectable (Fig. 1D and E).

Notably, the coefficient of variation (CV) for Venus-Us11 fluorescence intensities in each

infected cell was significantly higher than for TagRFP-ICP47 fluorescence (Fig. 1F).

To examine whether levels of Venus-Us11 fluorescence in rICP47/vUs11-

infected cells were related to those of the global expression of HSV-1 L proteins, HeLa

cells infected with rICP47/vUs11 at an MOI of 5 for 24 h were analyzed by flow cytometry and sorted into six subpopulations (f1 to f6) based on the levels of Venus-Us11 fluorescence intensities—Venus-Us11 fluorescence intensities increased in subpopulations from f1–f6 (S-Fig. 1A). The subpopulations were then subjected to LC-MS/MS to quantitate peptides of global HSV-1 L proteins (Fig. 2A and S-Fig. 1B). Among the HSV-1 L proteins detected (48 L proteins), there was a strong correlation between the levels of Venus-Us11 fluorescence intensity and the relative abundance of most HSV-1 L proteins including Venus-Us11 (33 L proteins,  $r > 0.90$ ,  $P < 0.001$ ; 10 L proteins,  $r > 0.70$ ,  $P < 0.01$ ; 4 L proteins,  $r > 0.58$ ,  $P < 0.05$ ) but not Us8.5 ( $r = 0.54$ ,  $P = 0.07$ ). These results suggested that Venus-Us11 fluorescence intensities reflected expression levels of global HSV-1 L proteins in rICP47/vUs11-infected cells.

**Specific Venus-Us11 protein expression levels are linked to progeny virus production.** To analyze a relationship between expression levels of HSV-1 L proteins and progeny virus yields directly and quantitatively, HeLa cells were infected with rICP47/vUs11 at an MOI of 5, harvested at 4, 6, 8, 10, 12, and 24 h after infection, analyzed by flow cytometry and sorted into entire population (FSC singlet) or six subpopulations (f1 to f6) according to the levels of Venus-Us11 fluorescence intensity

(S-Fig. 2). Virus titers in the entire population and each of the subpopulations were determined and virus titers per  $10^4$  cells were estimated.

In agreement with previous reports <sup>4,6</sup>, the kinetics of Venus-Us11 fluorescence intensity were similar to those of progeny virus titers (Fig. 3A) and Venus-Us11 fluorescence intensities had a high correlation with progeny virus titers at the entire population level ( $r=0.95$ ) (Fig. 3B). We also calculated virtual titers per  $10^4$  cells at each timepoint by summing virus titers in subpopulations, obtained by multiplying the estimated virus titer of each subpopulation of  $10^4$  cells by the ratio of number of cells in the subpopulation to that in the entire population. A viral growth curve based on the virtual titers was almost identical to that based on actual titers in the entire population (Fig. 3C).

At the entire population level, virus titers were decreased 6 h after infection due to an eclipse phase of infection and viral replication entered the productive phase between 6 and 8 h post-infection (Fig. 3A and C). These results indicated that infectious progeny virus production was detectable 8 h after infection in these experiments. The f4 subpopulation emerged at this timepoint (Fig. 3D, F and G, and S-Table 2). Although 4.1% of total cells were in the f4 subpopulation 8 h after infection (Fig. 3D, and S-Table 2), 55% of progeny infectious virus yields were produced by this subpopulation (Fig. 3E,

and S-Table 2). The f5 and f6 subpopulations emerged 10 and 12 h after infection, respectively, when the growth rate had slowed (Fig. 3D, F and G, and S-Table 2). At 10 h after infection, 18% of total cells were in the f4 and f5 subpopulations (Fig. 3D, and S-Table 2) and these subpopulations produced 87% of progeny infectious virus yields (Fig. 3E, and S-Table 2). At 12 and 24 h post-infection, 33% and 53% of total cells were in the f4 to f6 subpopulations, respectively (Fig. 3D, and S-Table 2), and these subpopulations produced 95% of progeny infectious virus yields (Fig. 3E, and S-Table 2). Similarly, most progeny infectious virus yields were produced by the f4 to f6 subpopulations in HeLa cells using MOIs of 1 and 2.5 at 24 h post-infection and in other cells (Vero, U2Os and HaCaT cells, and human fetal foreskin fibroblasts (HFFF-2)) at MOIs 1 or 2.5 at 12 h post-infection, although the proportion of each subpopulation varied by different MOI and cell type (S-Figs. 3A to D and 4A to D, F to I, K to N and P to S). Notably, the viral growth curve from 8 h post-infection based on the virtual titers using only the data of the f4 to f6 subpopulations was almost identical to that based on the virtual titers using the data of the f1 to f6 populations or actual titers of the entire population (Fig. 4A and B). Similarly, virtual titers using only the data of the f4 to f6 subpopulations in HeLa cells at MOIs of 1 and 2.5 and in Vero, U2OS, and HaCaT cells, and HFFF-2 were also similar to virtual titers using the data of f1 to f6 populations or actual titers in the entire population

(S-Figs. 3E to G, 4E, 4J, 4O, and 4T). These results indicated that subpopulations f4 to f6 have a predominant role in yielding progeny infectious viruses, whereas subpopulations f1 to f3 barely produced infectious virions. To obtain evidence to further support this conclusion, we analyzed virion morphogenesis by quantitating the number of virus particles at different morphogenetic stages in HSV-1-infected HeLa cells at an MOI of 5 for 8 (S-Fig. 5) or 24 h (Fig. 5) in each subpopulation f2 to f4 or f5, respectively, by electron microscopy. All virion types were barely detectable in infected cells from subpopulation f2 (Fig. 5 and S-Fig. 5). In subpopulation f3, although nuclear virions were obvious, cytoplasmic virions, and especially enveloped virions in the cytoplasm that were considered infectious, were barely detectable (Fig. 5 and S-Fig. 5). In contrast, enveloped virions were detected in the cytoplasm of 100% of infected cells in the f4 subpopulation at 8 h post-infection (S-Fig. 5) and these virions were detected in the cytoplasm of 70% and 100% of infected cells in the f4 and f5 subpopulations, respectively, at 24 h post-infection (Fig. 5). The proliferative profiles of enveloped virions in the cytoplasm (Fig. 5 and S-Fig. 5) were similar to those of infectious virus titers (S-Fig. 6A).

We noted that, even at 4 and 6 h post-infection, the virus titers in f1 to f3 subpopulations were detectable at a maximum of  $2.8 \times 10^2$  PFU/ $10^4$  cells (Fig. 3G and S-Table 2). Taken together with the series of observations above (Figs. 3D and E, 4A and

B, and 5, and S-Figs. 3, 4, 5, and 6A) indicating that infected cells in subpopulations f1 to f3 barely produced infectious virions, it was not likely that infectious virus titers in subpopulations f1 to f3 detected ranging from  $2.6 \times 10^1$  to  $9.3 \times 10^2$  PFU/ $10^4$  cells (Fig. 3G and S-Table 2) represented progeny virus yields of infected cells in f1 to f3 subpopulations. Cells in the f1 to f3 subpopulations were likely to be aborted infected cells and their frequencies 24 h after infection were similar to those reported previously in HeLa cells<sup>13,22</sup>.

Collectively, these results together with the observation that Venus-Us11 fluorescence intensities reflected the expression levels of global HSV-1 L proteins indicated that certain levels of L protein expression were required for progeny virus production and a threshold of progeny virus production existed between Venus-Us11 protein expression levels in subpopulations f3 and f4. Notably, Venus-Us11 fluorescence intensities in subpopulations above the threshold (f4 to f6) correlated highly with progeny virus titers ( $r=0.87$ ) (Fig. 4C). In contrast, a much lower correlation of coefficient ( $r=0.46$ ) was observed in subpopulations below the threshold (Fig. 4C). Furthermore, virus titers in subpopulations f4 to f6 remained unchanged during HSV-1 infection (Fig. 4D and S-Fig. 6B) indicating L protein expression levels in subpopulations above the threshold were tightly correlated with virus titers independent of the timepoint after infection. Thus,

infectious progeny virus production in the entire population over time depended on the proportion of these subpopulations in the entire population.

**Virion morphogenesis with a defect in the cleavage/packaging of HSV-1 DNA genome occurs in the subpopulation below the threshold for progeny virus production.** The threshold for progeny virus production detected between Venus-Us11 protein expression levels in subpopulations f3 and f4 suggested a rate-limiting viral step for progeny virus production. Conceivably, this defect(s) might be observed in subpopulations below the threshold (f1 to f3) but not in subpopulations above the threshold (f4 to f6). To clarify this rate-limiting viral step, we compared levels of HSV-1 DNA genome replication and global viral mRNA expression in subpopulations f1 to f6 by quantitative PCR and RNA sequencing, respectively. Amounts of HSV-1 genome DNA increased in the f1 subpopulation and almost reached a plateau between subpopulations f2 and f3 (S-Fig. 7A). Similar proliferative profiles were observed for expressions of each of the 73 HSV-1 mRNAs tested (S-Fig. 7B). Thus, we did not detect any rate-limiting effects of HSV-1 genome replication or viral mRNA expression associated with the threshold for progeny virus production.

Next, we visualized virion morphogenesis by electron microscopy focusing on the A, B and C capsids in the nucleus (Fig. 6 and S-Fig. 8). The A and B capsids are

221 incomplete structures resulting from problems in viral DNA genome retention in the  
222 capsids and packaging into the capsids, respectively <sup>23-25</sup>. C capsids are mature capsids  
223 (nucleocapsids) containing viral DNA genomes reported to be selectively exported to the  
224 cytoplasm <sup>26-29</sup>. B capsids accumulated aberrantly in subpopulation f3 and most (90.1%)  
225 nuclear capsids in this subpopulation were B capsids (Fig. 6 and S-Fig. 8). The frequency  
226 of B capsids in subpopulation f3 was significantly higher than in subpopulations f4 and  
227 f5 (Fig. 6B). In contrast, the frequency of C capsids in subpopulation f3 was significantly  
228 lower than in subpopulations f4 and f5 (Fig. 6B). In agreement with this and previous  
229 reports that C capsids are selectively exported to the cytoplasm <sup>26-29</sup>, the frequency of  
230 virions in the perinuclear space and cytoplasm in subpopulation f3 was significantly lower  
231 than in subpopulations f4 and f5 (Fig. 6C). The frequency of A capsids in subpopulation  
232 f3 was comparable to those in subpopulations f4 and f5 (Fig. 6B). The frequencies of each  
233 type of nuclear capsid in subpopulations f4 and f5 were similar to those reported  
234 previously in wild-type HSV-1-infected HeLa cells <sup>30</sup>. Furthermore, the aberrant  
235 accumulation of B capsids and lack of nuclear C capsids and virions in the perinuclear  
236 space and cytoplasm in subpopulation f3 were also observed at 8h post-infection (S-Figs.  
237 5 and 9). These features of subpopulation f3 were similar to the phenotypes of HSV-  
238 mutants with defective viral DNA genome cleavage/packaging including those lacking

the portal protein UL6, a terminase subunit (UL15, UL33 or UL28) or a minor capsid protein (UL17 or UL32)<sup>31-37</sup>.

Collectively, these results suggested that the cleavage/packaging of HSV-1 DNA genome was specifically down-regulated in subpopulations below the threshold and that this viral step was a rate-limiting step for progeny virus production.

**A subset of HSV-1 L proteins including components of viral terminase have unique protein expression profiles.** We compared global HSV-1 L protein abundance in each subpopulation by LC-MS/MS, and there was a strong correlation between the Venus-Us11 fluorescence intensities and relative abundance of most HSV-1 L proteins detected (Fig. 2B). Therefore, we focused on the abundance profiles of the bottom 10 HSV-1 L proteins with a relatively low correlation (Fig. 7A). The abundance profiles of several of these HSV-1 L proteins including UL25, UL3, UL4, UL33, Us10, and UL15 (Fig. 7A) differed from those of other HSV-1 L proteins whose abundance continuously increased in subpopulations f1 to f6 (S-Fig. 1B). The abundance of these L proteins in subpopulations f1 to f3 were very low and remained relatively constant, but were increased in subpopulations f4 to f6.

Next, to quantitatively evaluate the delayed increase in the abundance of L protein in the subpopulations, a four-parameter logistic regression was used for curve

fitting of these profiles 24 h after infection (S-Fig. 10). The x-axis value at which the y-axis value increased by  $\log_{10}2$  (2-fold increase in linear scale) from the starting point ( $x=0$ ) for each curve was defined as the threshold value (TV) (S-Fig. 10 and Fig. 7B). Fig. 7C shows the top 10 proteins with the highest TV identified in this analysis. Of particular interest, these included all the subunits of HSV-1 terminase including UL15, UL33, UL28 and the HSV-1 portal protein UL6, all of which were reported to be required for viral DNA genome cleavage/packaging<sup>31-34,36</sup>. These results indicated that the expressions of a fraction of L proteins including all the subunits of HSV-1 terminase and the viral portal protein lacked in subpopulations f1 to f3, unlike that of other L proteins, suggesting the expressions of the L proteins are somehow downregulated in subpopulations below the threshold.

## DISCUSSION

Single-cell analyses have identified new subpopulations of virus-infected cells with similar viral gene expression profiles<sup>15-17</sup>. However, the use of single-cell analyses to investigate both viral gene expression and progeny virus production is limited. Thus, single-cell analyses for both viral RNA synthesis and progeny virus production have been reported for some RNA viruses<sup>10,12,14</sup>; a recent study reported that influenza virus transcription and progeny virus production were poorly correlated at the single cell level<sup>14</sup>, and other studies did not focus on the relationship between viral transcription and virus progeny production at the single cell level<sup>10,12</sup>. Furthermore, protein expression and virus progeny production at the single-cell or subpopulation level have not been investigated to date. This study established a system to fractionate HSV-1-infected cells based on global HSV-1 L protein expression levels and to titrate progeny virus yields in these fractions. This established system enabled us to clarify, for the first time, the direct and quantitative relationship between viral protein expression and progeny virus yields, and the clarified relationship indicated a threshold for HSV-1 L protein expression levels for progeny virus production. Such a threshold has not been reported by classical time course studies of most viruses at the entire population level by analyzing the relationship between viral gene expression and progeny virus yield. In contrast, once the levels of HSV-1 L

protein expression exceeded the threshold, they were highly correlated with infectious progeny virus yields as reported by our (Fig. 3B) and other previous studies at the entire population level <sup>4,6</sup>.

The threshold clarified in this study led us to identify the HSV-1 genome DNA cleavage/packaging step was a rate-limiting step for progeny virus production. Supporting this, MS analysis of the global expression of HSV-1 L proteins at the subpopulation level showed the expression of a subset of HSV-1 L proteins including all components of viral terminase and portal protein lacked in subpopulations below the threshold. Conceivably, an anti-viral strategy targeting this bottleneck step for HSV-1 production might block progeny virus production effectively. HSV-1 genome DNA cleavage/packaging, which is largely mediated by a specific viral enzyme HSV-1 terminase, is essential for viral replication <sup>31,33,34,36</sup>, and most targets of antiviral drugs successfully developed to date are viral specific enzymes <sup>38</sup>. Our study at the subpopulation level using this newly established system revealed an ideal target for the development of anti-viral drugs. Notably, the newly established system is simple and widely applicable for studies of the direct relationship between viral gene expression and progeny virus yield of many other DNA and RNA viruses, which might provide specific and conserved insights into mechanisms of progeny virus production in these viruses. It

will be particularly interesting to determine whether the rate-limiting step identified in the progeny virus production of HSV-1 is conserved in adenoviruses, which seem to utilize similar DNA genome packaging systems<sup>39</sup>.

It has long been recognized that much fewer virions are present in the cytoplasm of HSV-1-infected cells compared with the nucleus<sup>40-42</sup>. Our conclusion that the HSV-1 genome DNA cleavage/packaging step is a rate-limiting step for progeny virus production is in agreement with these observations as well as earlier reports demonstrating C capsids are selectively exported to the cytoplasm<sup>26-29</sup>. The rate-limiting step identified in this study also suggests a sophisticated strategy of efficient progeny virus production by HSV-1 without accumulating progeny nucleocapsids in the cytoplasm, which enables evasion from cytosolic sensors related to innate immune responses. In the cytoplasm, HSV-1 nucleocapsids are degraded by proteasomes<sup>43</sup>, and viral DNAs are likely to be sensed by cytosolic sensors including cGAS, AIM2, DAI, and RNA polymerase III, which promote innate immune responses<sup>44-49</sup>. Here we showed that, in subpopulation f3, which was likely slightly below the threshold, HSV-1 genome DNA replication had already reached a plateau and B capsid formation was easily observed although C capsid formation was barely detectable. In contrast, in subpopulation f4, which was likely slightly over the threshold, C capsids and all types of virions in the perinuclear space and the cytoplasm

were evident. These observations suggested that downregulating the HSV-1 DNA cleavage/packaging might promote the accumulation of nucleocapsid components including capsids and viral genome DNAs in the nucleus as well as other viral proteins required for virion maturation at the NMs and in the cytoplasm at a level sufficient for efficient progeny virus production. Once the viral genome is packaged into a capsid, the following steps for virion maturation might immediately proceed without accumulating any excess nucleocapsids in the cytoplasm, decreasing the chance for HSV-1 to be sensed by innate immune responses in the cytoplasm. IFI16 and hnRNPA2B1 sense HSV-1 genome DNA and promote innate immune responses in the nucleus<sup>50-52</sup>. However, replicated HSV-1 genome DNAs and nucleocapsids appear to accumulate in the nucleus of HSV-1-infected cells<sup>19,53,54</sup>, suggesting this virus has evolved more effective evasion mechanisms against innate immune responses in the nucleus such that ICP0 counteracts IFI16<sup>50</sup> and probably, against capsid degradation than those in the cytoplasm.

We noted that overall viral mRNA levels increased from the f1 subpopulation and almost reached a plateau between subpopulations f2 and f3 (S-Fig. 4B). In contrast, viral L protein levels continued to increase from the f1 to f6 subpopulations (S-Fig. 1B). Thus, there was a lack of correlation between viral L mRNA levels and viral L protein levels especially in fractions f4 to f6. In agreement with these observations, previous

341 systematic studies quantifying mRNA and protein levels at the genomic scale reported  
342 the importance of multiple processes beyond the mRNA concentration that contributed to  
343 establishing the level of a protein <sup>55</sup>. These processes include translation rates, translation  
344 rate modulation, modulation of a protein's stability, protein synthesis delay, and protein  
345 transport <sup>55</sup>. Interestingly, it was reported that HSV-1 VP22 promoted global viral protein  
346 expression <sup>56,57</sup>, potentially by reducing the dependence of protein synthesis upon cellular  
347 ribosomal proteins to support translation during infection <sup>58</sup>, and by promoting the  
348 translocation of viral L mRNAs to the cytoplasm <sup>59</sup>. HSV-1 might evolve VP22 to  
349 promote global viral translation efficiency in specific circumstances such as in  
350 subfractions f4 to f6, in which amounts of viral mRNAs are saturated.  
351

## MATERIALS AND METHODS

**Cells and Viruses.** HeLa, U2OS, HFFF-2, HaCaT, and Vero cells were described previously<sup>20,60</sup>. Wild-type HSV-1(F) was described previously<sup>61</sup>.

**Generation of a recombinant virus.** Recombinant virus YK410 (rICP47/vUs11) in which ICP47 and Us11 were tagged with TagRFP<sup>62</sup> and VenusA206K<sup>63</sup>, respectively, were generated by two rounds of two-step Red-mediated mutagenesis using *Escherichia coli* GS1783 containing pYEbac102Cre<sup>61,64</sup>, a full-length infectious HSV-1(F) clone, pBS-Venus-KanS<sup>20</sup>, pFlag-TagRFP-KanS, and the primers listed in S-Table 1. The viruses used in this study were propagated and titrated in Vero cells.

**Plasmids.** pFlag-TagRFP was constructed by amplifying the TagRFP open reading frame (ORF) to introduce a *KpnI* site without changing the amino acid sequence by PCR from pTagRFP-N1<sup>65</sup> and cloning it into pFlag-CMV2 (Sigma). pFlag-TagRFP-KanS, used in the two-step Red-mediated mutagenesis procedure, was constructed by amplifying the domain of pEP-KanS<sup>66</sup> carrying the *I-SceI* site and the kanamycin resistance gene by PCR from pEP-KanS using the primers 5'-GCGGTACCGTGAACAACCACCACTTCAAAGGATGACGACGATAAGTAGGG-3' and 5'-

GCGGTACCCTCCATGTACAGCTTCATGTCAACCAATTAACCAATTCTGATTA

G-3' and cloning it into the *KpnI* site of pFlag-TagRFP. pGEX-ICP47 was constructed by amplifying the ICP47 ORF by PCR from the HSV-1(F) genome and cloning it into pGEX-4T-1.

**Antibodies.** Commercial antibodies used in this study included mouse monoclonal antibody to  $\alpha$ -tubulin (DM1A; Sigma), and rabbit monoclonal antibodies to GFP (598; MBL) and TagRFP (AB233; Evrogen). Rabbit polyclonal antibodies to US11 were described previously<sup>41</sup>. To generate a rabbit polyclonal antibody to ICP47, a rabbit was immunized, according to the standard protocol at MBL, with GST-ICP47 expressed in *E. coli* and purified as described previously<sup>20</sup>. Serum from the immunized rabbit was used as the anti-ICP47 polyclonal antibody.

**Immunoblotting.** Immunoblotting was performed as described previously<sup>67</sup>.

**Flow cytometry.** HeLa cells infected with HSV-1(F) or YK410 (rICP47/vUs11) were washed with phosphate buffered saline (PBS) and detached with 0.25% trypsin/EDTA solution (Wako). Then, the cells were suspended in PBS containing 2% FCS, filtered through a 35- $\mu$ m pore-cell strainer (#352235, Corning) and subjected to FACS analysis with BD FACS Melody (Becton Dickinson). The data were analyzed with BD FACSCorus (Becton Dickinson) software or FlowJo 10.8.1 software (Becton Dickinson).

### **Determination of viral titer in cells fractionated by cell sorting.** HeLa cells

were infected with YK410 (rICP47/vUs11) at an MOI of 5. At the indicated times after infection, cells were detached and suspended as described above. Then,  $1.5 \times 10^4$  to  $3 \times 10^4$  cells in the f1 to f6 subpopulations, and the entire cell population (FSC-singlet), were sorted into medium 199 containing 1% FCS by FACS Melody (Becton Dickinson). The sorted cells were freeze-thawed once, sonicated, and virus titers were determined by plaque assay using Vero cells. The average virus titer per single cell was obtained by dividing the obtained virus titer by the number of sorted cells. Data are presented as the PFU per  $10^4$  cells.

### **Calculation of the proportion of virus titers in each subpopulation and the**

**virtual titer.**  $\text{PFU}_{fi}$ , which represents the viral titer of each subpopulation  $fi$  ( $i = 1$  to 6), was obtained using the following equation:

$$\text{PFU}_{fi} = \text{PFU}_{fi/\text{cell}} \times 10^4 \times \text{PR}_{fi} / 100$$

where  $\text{PFU}_{fi/\text{cell}}$  is the average viral titer per single cell belonging to the  $fi$  subpopulation (from Fig. 3F and G) and  $\text{PR}_{fi}$  is the proportion (%) of cells in the  $fi$  fraction in the entire population (from Fig. 3D). The virtual titer (VT), which represents the sum of  $\text{PFU}_{fi}$  was obtained as follows:

$$\text{VT} = \text{PFU}_{f1} + \text{PFU}_{f2} + \text{PFU}_{f3} + \text{PFU}_{f4} + \text{PFU}_{f5} + \text{PFU}_{f6}$$

406 % of PFU<sub>Pi</sub>, which represents the proportion of viral titers in the f<sub>i</sub> subpopulation  
 407 accounted for in the entire population (Fig. 3E) was obtained using the following  
 408 equation:

$$409 \quad \% \text{ of PFU}_{f_i} = \text{PFU}_{f_i} / \text{VT} \times 100$$

410 **LC-MS/MS analysis of cells fractionated by cell sorting.** HeLa cells were  
 411 infected with rICP47/vUs11 at an MOI of 5 for 24 h. Then, cells were detached and  
 412 suspended as described above. Next, 10<sup>5</sup> cells in the f<sub>1</sub> to f<sub>6</sub> subpopulation were sorted  
 413 into PBS by BD FACS Melody (Becton Dickinson), pelleted by centrifugation, and lysed  
 414 with lysis buffer (0.1 M of Tris-HCl (pH 8.0), 1% SDS). To remove SDS from samples,  
 415 we used the methanol-chloroform protein precipitation method. Briefly, we added 4  
 416 volumes of methanol, 1 volume of chloroform, and 3 volumes of water to the eluted  
 417 sample and mixed thoroughly. The samples were centrifuged at 15,000 rpm for 10 min,  
 418 the water phase was carefully removed, and then 4 volumes of methanol were added to  
 419 the samples. The samples were centrifuged at 15,000 rpm for 10 min, and the supernatant  
 420 was removed. The pellet was washed once with 100% ice-cold acetone. The precipitated  
 421 protein was re-dissolved in guanidine hydrochloride, reduced with TCEP, alkylated with  
 422 iodoacetamide, and digested with lysyl endopeptidase and trypsin. The resulting digested  
 423 peptides were analyzed using an Evosep One LC system (EVOSEP) connected to a Q-

Exactive HF-X mass spectrometer (Thermo) with a Dream spray tip (AMR) and a 15 cm × 150 µm column packed with 1.9-µm C18-beads (Evosep). The mobile phases were comprised of 0.1% FA as solution A and 0.1% FA/99.9% ACN as solution B. The analysis was performed in the data-dependent acquisition mode, where the top 25 recorded mass spectrometry spectra between 380 and 1500 m/z were selected. Survey scans were acquired at a resolution of 60,000 at m/z 200, and the tandem mass spectrometry (MS/MS) resolution was set to 15,000 at m/z 200. All MS/MS spectra were searched against the protein sequences of the HSV protein database and human Swiss-Prot database using Proteome Discoverer 2.2 (Thermo) with the SEQUEST search engine, and the result of HSV proteins was extracted. The false discovery rate (FDR) was set to 1% on peptide spectrum match (PSM).

**Data processing of LC-MS/MS data.** Normalization was performed on quantitative values using the method built into the Discoverer 2.2 software. Briefly, the Total Peptide Amount mode was used to normalize between samples, and the On All Average mode was used to normalize between identified proteins. The subsequent analysis was performed using only the extracted data for HSV proteins. The normalization method in each mode was as follows. The Total Peptide Amount mode sums the peptide group abundances for each sample and determines the maximum sum

for all files. The normalization factor is the factor of the sum of the samples and the maximum sum in all files. The On All Average mode aggregates all the abundance or normalized abundance values per sample and scales the abundance values of each sample so that the average of all samples is 100. When a peptide was not detected in four technical replicates from one sample of each subpopulation, the protein was considered undetectable in that subpopulation. When a peptide was not detected in a replicate of each subpopulation, the missing value was complemented with the mean value of abundances in technical replicates where the peptide was detected. The mean value of abundances from four technical replicates were used as the value of a single experiment. The relative abundance of each HSV-1 L protein was calculated relative to the subpopulation with the lowest mean abundance for two biologically independent experiments as 1.

#### **RNA-sequencing in cells fractionated by cell sorting.** HeLa cells were

infected with YK410 (rICP47/vUs11) at an MOI of 5 for 24 h. Then, cells were detached and suspended as described above. Next,  $5 \times 10^5$  cells in the f1 to f6 subpopulations were sorted into PBS by BD FACS Melody (Becton Dickinson). After centrifugation, total RNA from fractionated cells was isolated with a High Pure RNA Isolation kit (Roche). (i) Each cDNA was generated using a Clontech SMART-Seq HT Kit (Takara Clontech, Mountain View, CA, USA), and each library was prepared using a Nextera XT DNA

Library Prep Kit (Illumina, San Diego, USA). Sequencing was performed on the DNBSEQ-G400 platform in the 100+100-base paired-end mode. (ii) Generated reads were a mixture of human reads and HSV-1 reads. For human data, generated reads were mapped to the human (hg19) reference genome using TopHat v2.1.1 combined with Bowtie2 ver. 2.2.8 and SAMtools ver. 0.1.18. For HSV-1, generated reads were mapped to the HSV-1 (GenBank: GU734771.1) reference genome using HISAT2 v2.1.0. (iii) The quantification to obtain the read counts of each gene from HSV-1 was performed using featureCounts of subread-2.0.0 with option -M --fraction. With the length data of each gene (another output of the featureCounts), fragments per kilobase of exon per million mapped fragments (FPKMs) were calculated according to the definition. The FPKM of HSV-1 genes was multiplied by (total number of mapped reads of the HSV-1 genome)/{(total number of mapped reads of the human genome) + (total number of mapped reads of the HSV-1 genome)}, normalized by the amount relative to the value of the f1 fraction.

#### **Quantification of HSV-1 DNA in cells fractionated by cell sorting.**

HeLa cells were infected with YK410 (rICP47/vUs11) at an MOI of 5 for 24 h. Then, cells were detached and suspended as described above. Next,  $5 \times 10^4$  cells in the f1 to f6 subpopulations were sorted into PBS by BD FACS Melody (Becton Dickinson). After

centrifugation, total DNA from fractionated cells was isolated with NucleoSpin Tissue XS (TAKARA) according to the manufacturer's instructions. The amount of HSV-1 DNA was quantified using the Universal Probe Library (Roche) with TaqMan Master (Roche) and the LightCycler 96 System (Roche) according to the manufacturer's instructions. Primers and probes were designed using probe finder software within the region encoding ICP27 in the HSV-1 genome, and within the region encoding 18S rRNA in the human genome. The primer and probe sequences for ICP27 (for HSV-1 DNA) were 5'-TCCGACAGCGATCTGGAC-3', 5'-TCCGACGAGGAACACTCC-3', and Universal ProbeLibrary probe 56, and for 18S rRNA (for human DNA) the sequences were 5'-GCAATTATTCCCCATGAACG-3', 5'-GGGACTTAATCAACGCAAGC-3', and Universal ProbeLibrary probe 48. The  $\Delta C_t$  was calculated by subtracting the  $C_t$  value of HSV-1 DNA by the  $C_t$  value of human DNA. The relative amount of HSV-1 DNA to human DNA ( $2^{-\Delta C_t}$ ) was normalized relative to the value of the f1 subpopulation.

#### **Electron microscopic analysis of cells fractionated by cell sorting.**

HeLa cells were infected with YK410 (rICP47/vUs11) at an MOI of 5 for 8 h or 24 h. Then, cells were detached and suspended as described above. Next,  $5 \times 10^5$  to  $1 \times 10^6$  cells in the f2 to f4 (8 h) or f2 to f5 (24 h) subpopulations were sorted by BD FACS Melody (Becton Dickinson). After centrifugation, the pelleted cells were examined by ultrathin-section

electron microscopy as described previously<sup>68</sup> except using JEM-1400 Flash microscope (JEOL).

**Statistical analysis.** The unpaired Student's *t*-test was used to compare two groups. One-way ANOVA followed by the Tukey multiple comparisons test, or Mann-Whitney *U*-test followed by Bonferroni correction were used for multiple comparisons. A P-value < 0.05 was considered statistically significant. For the statistical comparison of viral titers, data were converted to common logarithms (log<sub>10</sub>). Pearson correlation coefficients (*r*) and *p*-values were calculated on log<sub>10</sub> transformed data. GraphPad Prism 10 (GraphPad Software) was used to perform statistical analyses.

**Classification of HSV-1 genes.** HSV-1 genes were classified into IE, E, and L genes as described previously<sup>19</sup>.

**Curve fitting.** To describe the abundance profiles of HSV-1 L proteins, we mainly used the following mathematical model developed by dose response modeling<sup>69</sup>.

$$f(x) = c + \frac{d - c}{1 + \exp(b(x - a))} \quad (1)$$

The variable  $f(x)$  is the abundance profiles of HSV-1 L proteins. The parameter  $a$  is the inflection point of the curve for this model, that is, the point where a change in acceleration in the curve occurs. The parameter  $b$  is a slope parameter and the

513 parameters  $c$  and  $d$  are the lower and upper horizontal asymptotes or limits,

514 respectively.

515 Fitting was performed by drc package in R, which estimates the parameters with

516 nonlinear least squares under the assumption of normally distributed response values <sup>70</sup>.

517

# REFERENCES

1. Whelan, S. (2013). Viral Replication Strategies. In Fields virology, D.M. Knipe, P.M. Howley, J.I. Cohen, D.E. Griffin, R.A. Lamb, M.A. Martin, V.R. Racaniello, and B. Roizman, eds. (Lippincott-Williams & Wilkins), pp. 105-126.
2. Brown, D.M., Kauder, S.E., Cornell, C.T., Jang, G.M., Racaniello, V.R., and Semler, B.L. (2004). Cell-dependent role for the poliovirus 3' noncoding region in positive-strand RNA synthesis. *J Virol* *78*, 1344-1351. 10.1128/jvi.78.3.1344-1351.2004.
3. Kim, D., Kim, S., Park, J., Chang, H.R., Chang, J., Ahn, J., Park, H., Park, J., Son, N., Kang, G., et al. (2021). A high-resolution temporal atlas of the SARS-CoV-2 translatome and transcriptome. *Nat Commun* *12*, 5120. 10.1038/s41467-021-25361-5.
4. Lloyd, M.G., Yee, M.B., Flot, J.S., Liu, D., Geiler, B.W., Kinchington, P.R., and Moffat, J.F. (2022). Development of Robust Varicella Zoster Virus Luciferase Reporter Viruses for In Vivo Monitoring of Virus Growth and Its Antiviral Inhibition in Culture, Skin, and Humanized Mice. *Viruses* *14*. 10.3390/v14040826.
5. Ouwendijk, W.J.D., Dekker, L.J.M., van den Ham, H.J., Lenac Rovis, T., Haefner, E.S., Jonjic, S., Haas, J., Luider, T.M., and Verjans, G. (2020). Analysis of Virus and Host Proteomes During Productive HSV-1 and VZV Infection in Human Epithelial Cells. *Front Microbiol* *11*, 1179. 10.3389/fmicb.2020.01179.
6. Tamura, T., Fukuhara, T., Uchida, T., Ono, C., Mori, H., Sato, A., Fauzyah, Y., Okamoto, T., Kurosu, T., Setoh, Y.X., et al. (2018). Characterization of Recombinant

539 Flaviviridae Viruses Possessing a Small Reporter Tag. *J Virol* *92*, 10.1128/JVI.01582-  
540 17.

541 7. Delbruck, M. (1945). The burst size distribution in the growth of bacterial viruses  
542 (bacteriophages). *J Bacteriol* *50*, 131-135. 10.1128/JB.50.2.131-135.1945.

543 8. Zhu, Y., Yongky, A., and Yin, J. (2009). Growth of an RNA virus in single cells reveals  
544 a broad fitness distribution. *Virology* *385*, 39-46. 10.1016/j.virol.2008.10.031.

545 9. Timm, A., and Yin, J. (2012). Kinetics of virus production from single cells. *Virology*  
546 *424*, 11-17. 10.1016/j.virol.2011.12.005.

547 10. Schulte, M.B., and Andino, R. (2014). Single-cell analysis uncovers extensive  
548 biological noise in poliovirus replication. *J Virol* *88*, 6205-6212. 10.1128/JVI.03539-  
549 13.

550 11. Combe, M., Garijo, R., Geller, R., Cuevas, J.M., and Sanjuan, R. (2015). Single-Cell  
551 Analysis of RNA Virus Infection Identifies Multiple Genetically Diverse Viral  
552 Genomes within Single Infectious Units. *Cell Host Microbe* *18*, 424-432.  
553 10.1016/j.chom.2015.09.009.

554 12. Heldt, F.S., Kupke, S.Y., Dorl, S., Reichl, U., and Frensing, T. (2015). Single-cell  
555 analysis and stochastic modelling unveil large cell-to-cell variability in influenza A  
556 virus infection. *Nat Commun* *6*, 8938. 10.1038/ncomms9938.

557 13. Wildy, P., Stoker, M.G.P., and Ross, R.W. (1959). Release of Herpes Virus from  
558 Solitary HeLa Cells. *Journal of General Microbiology* *20*, 105-112. 10.1099/00221287-  
559 20-1-105.

- 560 14. Bacsik, D.J., Dadonaite, B., Butler, A., Greaney, A.J., Heaton, N.S., and Bloom, J.D.  
561 (2023). Influenza virus transcription and progeny production are poorly correlated in  
562 single cells. *Elife* 12. 10.7554/eLife.86852.
- 563 15. Drayman, N., Patel, P., Vistain, L., and Tay, S. (2019). HSV-1 single-cell analysis  
564 reveals the activation of anti-viral and developmental programs in distinct sub-  
565 populations. *Elife* 8. 10.7554/eLife.46339.
- 566 16. Ku, C., Sheyn, U., Sebe-Pedros, A., Ben-Dor, S., Schatz, D., Tanay, A., Rosenwasser,  
567 S., and Vardi, A. (2020). A single-cell view on alga-virus interactions reveals  
568 sequential transcriptional programs and infection states. *Sci Adv* 6, eaba4137.  
569 10.1126/sciadv.aba4137.
- 570 17. Suomalainen, M., and Greber, U.F. (2021). Virus Infection Variability by Single-Cell  
571 Profiling. *Viruses* 13. 10.3390/v13081568.
- 572 18. Knipe, D.M., Heldwein, E.E., Mohr, I.J., Sodroski, C.N., Whitley, R.J., and Johnston,  
573 C. (2022). Herpes Simplex Viruses: Pathogenesis and Clinical Insights. In *Fields*  
574 *virology*, P.M. Howley, D.M. Knipe, B. Damania, J.I. Cohen, S.P.J. Whelan, E.O.  
575 Freed, and L. Enquist, eds. (Lippincott-Williams & Wilkins), pp. 297-323.
- 576 19. Roizman, B., Knipe, D.M., and Whitley, R.J. (2013). Herpes simplex viruses. In *Fields*  
577 *virology*, D.M. Knipe, P.M. Howley, J.I. Cohen, D.E. Griffin, R.A. Lamb, M.A. Martin,  
578 V.R. Racaniello, and B. Roizman, eds. (Lippincott-Williams & Wilkins), pp. 1823-  
579 1897.
- 580 20. Kato, A., Adachi, S., Kawano, S., Takeshima, K., Watanabe, M., Kitazume, S., Sato,  
581 R., Kusano, H., Koyanagi, N., Maruzuru, Y., et al. (2020). Identification of a herpes

582 simplex virus 1 gene encoding neurovirulence factor by chemical proteomics. Nat  
583 Commun *11*, 4894. 10.1038/s41467-020-18718-9.

584 21. Whisnant, A.W., Jurgens, C.S., Hennig, T., Wyler, E., Prusty, B., Rutkowski, A.J.,  
585 L'Hernault, A., Djakovic, L., Gobel, M., Doring, K., et al. (2020). Integrative  
586 functional genomics decodes herpes simplex virus 1. Nat Commun *11*, 2038.  
587 10.1038/s41467-020-15992-5.

588 22. Cohen, E.M., Avital, N., Shamay, M., and Kobiler, O. (2020). Abortive herpes simplex  
589 virus infection of nonneuronal cells results in quiescent viral genomes that can  
590 reactivate. Proc Natl Acad Sci U S A *117*, 635-640. 10.1073/pnas.1910537117.

591 23. Cardone, G., Heymann, J.B., Cheng, N., Trus, B.L., and Steven, A.C. (2012).  
592 Procapsid assembly, maturation, nuclear exit: dynamic steps in the production of  
593 infectious herpesvirions. Adv Exp Med Biol *726*, 423-439. 10.1007/978-1-4614-0980-  
594 9\_19.

595 24. Homa, F.L. (1997). Capsid assembly and DNA packaging in herpes simplex virus.  
596 Reviews in medical virology *7*, 107-122.

597 25. Baines, J.D. (2011). Herpes simplex virus capsid assembly and DNA packaging: a  
598 present and future antiviral drug target. Trends Microbiol *19*, 606-613.  
599 10.1016/j.tim.2011.09.001.

600 26. Takeshima, K., Arii, J., Maruzuru, Y., Koyanagi, N., Kato, A., and Kawaguchi, Y.  
601 (2019). Identification of the Capsid Binding Site in the Herpes Simplex Virus 1  
602 Nuclear Egress Complex and Its Role in Viral Primary Envelopment and Replication.  
603 J Virol *93*. 10.1128/JVI.01290-19.

- 604 27. Yang, K., and Baines, J.D. (2011). Selection of HSV capsids for envelopment involves  
605 interaction between capsid surface components pUL31, pUL17, and pUL25. *Proc*  
606 *Natl Acad Sci U S A* *108*, 14276-14281. 10.1073/pnas.1108564108.
- 607 28. Yang, K., Wills, E., Lim, H.Y., Zhou, Z.H., and Baines, J.D. (2014). Association of  
608 herpes simplex virus pUL31 with capsid vertices and components of the capsid  
609 vertex-specific complex. *J Virol* *88*, 3815-3825. 10.1128/JVI.03175-13.
- 610 29. Johnson, D.C., and Baines, J.D. (2011). Herpesviruses remodel host membranes for  
611 virus egress. *Nat Rev Microbiol* *9*, 382-394. 10.1038/nrmicro2559.
- 612 30. Khadivjam, B., Bonneil, E., Thibault, P., and Lippe, R. (2023). RNA helicase DDX3X  
613 modulates herpes simplex virus 1 nuclear egress. *Commun Biol* *6*, 134.  
614 10.1038/s42003-023-04522-w.
- 615 31. Heming, J.D., Conway, J.F., and Homa, F.L. (2017). Herpesvirus Capsid Assembly  
616 and DNA Packaging. *Adv Anat Embryol Cell Biol* *223*, 119-142. 10.1007/978-3-319-  
617 53168-7\_6.
- 618 32. Patel, A.H., Rixon, F.J., Cunningham, C., and Davison, A.J. (1996). Isolation and  
619 characterization of herpes simplex virus type 1 mutants defective in the UL6 gene.  
620 *Virology* *217*, 111-123. 10.1006/viro.1996.0098.
- 621 33. Baines, J.D., Cunningham, C., Nalwanga, D., and Davison, A. (1997). The U(L)15  
622 gene of herpes simplex virus type 1 contains within its second exon a novel open  
623 reading frame that is translated in frame with the U(L)15 gene product. *J Virol* *71*,  
624 2666-2673. 10.1128/JVI.71.4.2666-2673.1997.

- 625 34. Yang, K., Dang, X., and Baines, J.D. (2017). A Domain of Herpes Simplex Virus  
626 pU(L)33 Required To Release Monomeric Viral Genomes from Cleaved Concatemeric  
627 DNA. *J Virol* 91. 10.1128/JVI.00854-17.
- 628 35. Salmon, B., Cunningham, C., Davison, A.J., Harris, W.J., and Baines, J.D. (1998).  
629 The herpes simplex virus type 1 U(L)17 gene encodes virion tegument proteins that  
630 are required for cleavage and packaging of viral DNA. *J Virol* 72, 3779-3788.  
631 10.1128/JVI.72.5.3779-3788.1998.
- 632 36. Tengelsen, L.A., Pederson, N.E., Shaver, P.R., Wathen, M.W., and Homa, F.L. (1993).  
633 Herpes simplex virus type 1 DNA cleavage and encapsidation require the product of  
634 the UL28 gene: isolation and characterization of two UL28 deletion mutants. *J Virol*  
635 67, 3470-3480. 10.1128/JVI.67.6.3470-3480.1993.
- 636 37. Lamberti, C., and Weller, S.K. (1998). The herpes simplex virus type 1  
637 cleavage/packaging protein, UL32, is involved in efficient localization of capsids to  
638 replication compartments. *J Virol* 72, 2463-2473. 10.1128/JVI.72.3.2463-2473.1998.
- 639 38. Tompa, D.R., Immanuel, A., Srikanth, S., and Kadhirvel, S. (2021). Trends and  
640 strategies to combat viral infections: A review on FDA approved antiviral drugs. *Int*  
641 *J Biol Macromol* 172, 524-541. 10.1016/j.ijbiomac.2021.01.076.
- 642 39. Ahi, Y.S., and Mittal, S.K. (2016). Components of Adenovirus Genome Packaging.  
643 *Front Microbiol* 7, 1503. 10.3389/fmicb.2016.01503.
- 644 40. Lymberopoulos, M.H., Bourget, A., Ben Abdeljelil, N., and Pearson, A. (2011).  
645 Involvement of the UL24 protein in herpes simplex virus 1-induced dispersal of B23  
646 and in nuclear egress. *Virology* 412, 341-348. 10.1016/j.virol.2011.01.016.

647 41. Takeshima, K., Maruzuru, Y., Koyanagi, N., Kato, A., and Kawaguchi, Y. (2022).  
648 Redundant and Specific Roles of A-Type Lamins and Lamin B Receptor in Herpes  
649 Simplex Virus 1 Infection. *J Virol* *96*, e0142922. 10.1128/jvi.01429-22.

650 42. Hutchinson, L., and Johnson, D.C. (1995). Herpes simplex virus glycoprotein K  
651 promotes egress of virus particles. *J Virol* *69*, 5401-5413. 10.1128/JVI.69.9.5401-  
652 5413.1995.

653 43. Horan, K.A., Hansen, K., Jakobsen, M.R., Holm, C.K., Soby, S., Unterholzner, L.,  
654 Thompson, M., West, J.A., Iversen, M.B., Rasmussen, S.B., et al. (2013). Proteasomal  
655 degradation of herpes simplex virus capsids in macrophages releases DNA to the  
656 cytosol for recognition by DNA sensors. *J Immunol* *190*, 2311-2319.  
657 10.4049/jimmunol.1202749.

658 44. Chiu, Y.H., Macmillan, J.B., and Chen, Z.J. (2009). RNA polymerase III detects  
659 cytosolic DNA and induces type I interferons through the RIG-I pathway. *Cell* *138*,  
660 576-591. 10.1016/j.cell.2009.06.015.

661 45. Takaoka, A., Wang, Z., Choi, M.K., Yanai, H., Negishi, H., Ban, T., Lu, Y., Miyagishi,  
662 M., Kodama, T., Honda, K., et al. (2007). DAI (DLM-1/ZBP1) is a cytosolic DNA sensor  
663 and an activator of innate immune response. *Nature* *448*, 501-505.  
664 10.1038/nature06013.

665 46. Sun, L., Wu, J., Du, F., Chen, X., and Chen, Z.J. (2013). Cyclic GMP-AMP synthase  
666 is a cytosolic DNA sensor that activates the type I interferon pathway. *Science* *339*,  
667 786-791. 10.1126/science.1232458.

668 47. Li, X.D., Wu, J., Gao, D., Wang, H., Sun, L., and Chen, Z.J. (2013). Pivotal roles of  
669 cGAS-cGAMP signaling in antiviral defense and immune adjuvant effects. *Science*  
670 *341*, 1390-1394. 10.1126/science.1244040.

671 48. Maruzuru, Y., Ichinohe, T., Sato, R., Miyake, K., Okano, T., Suzuki, T., Koshiba, T.,  
672 Koyanagi, N., Tsuda, S., Watanabe, M., et al. (2018). Herpes Simplex Virus 1 VP22  
673 Inhibits AIM2-Dependent Inflammasome Activation to Enable Efficient Viral  
674 Replication. *Cell Host Microbe* *23*, 254-265 e257. 10.1016/j.chom.2017.12.014.

675 49. Lee, S., Karki, R., Wang, Y., Nguyen, L.N., Kalathur, R.C., and Kanneganti, T.D.  
676 (2021). AIM2 forms a complex with pyrin and ZBP1 to drive PANoptosis and host  
677 defence. *Nature* *597*, 415-419. 10.1038/s41586-021-03875-8.

678 50. Orzalli, M.H., DeLuca, N.A., and Knipe, D.M. (2012). Nuclear IFI16 induction of IRF-  
679 3 signaling during herpesviral infection and degradation of IFI16 by the viral ICP0  
680 protein. *Proc Natl Acad Sci U S A* *109*, E3008-3017. 10.1073/pnas.1211302109.

681 51. Li, T., Diner, B.A., Chen, J., and Cristea, I.M. (2012). Acetylation modulates cellular  
682 distribution and DNA sensing ability of interferon-inducible protein IFI16. *Proc Natl*  
683 *Acad Sci U S A* *109*, 10558-10563. 10.1073/pnas.1203447109.

684 52. Wang, L., Wen, M., and Cao, X. (2019). Nuclear hnRNPA2B1 initiates and amplifies  
685 the innate immune response to DNA viruses. *Science* *365*. 10.1126/science.aav0758.

686 53. Morgan, C., Ellison, S.A., Rose, H.M., and Moore, D.H. (1954). Structure and  
687 development of viruses as observed in the electron microscope. I. Herpes simplex  
688 virus. *J Exp Med* *100*, 195-202. 10.1084/jem.100.2.195.

689 54. de Bruyn Kops, A., and Knipe, D.M. (1988). Formation of DNA replication structures  
690 in herpes virus-infected cells requires a viral DNA binding protein. *Cell* *55*, 857-868.  
691 10.1016/0092-8674(88)90141-9.

692 55. Liu, Y., Beyer, A., and Aebersold, R. (2016). On the Dependency of Cellular Protein  
693 Levels on mRNA Abundance. *Cell* *165*, 535-550. 10.1016/j.cell.2016.03.014.

694 56. Duffy, C., Mbong, E.F., and Baines, J.D. (2009). VP22 of herpes simplex virus 1  
695 promotes protein synthesis at late times in infection and accumulation of a subset of  
696 viral mRNAs at early times in infection. *J Virol* *83*, 1009-1017. 10.1128/JVI.02245-  
697 07.

698 57. Tanaka, M., Kato, A., Satoh, Y., Ide, T., Sagou, K., Kimura, K., Hasegawa, H., and  
699 Kawaguchi, Y. (2012). Herpes simplex virus 1 VP22 regulates translocation of  
700 multiple viral and cellular proteins and promotes neurovirulence. *J Virol* *86*, 5264-  
701 5277. 10.1128/JVI.06913-11.

702 58. Vink, E.I., Andrews, J., Duffy, C., and Mohr, I. (2021). Preventing translational  
703 inhibition from ribosomal protein insufficiency by a herpes simplex virus-encoded  
704 ribosome-associated protein. *Proc Natl Acad Sci U S A* *118*. 10.1073/pnas.2025546118.

705 59. Pheasant, K., Moller-Levet, C.S., Jones, J., Depledge, D., Breuer, J., and Elliott, G.  
706 (2018). Nuclear-cytoplasmic compartmentalization of the herpes simplex virus 1  
707 infected cell transcriptome is co-ordinated by the viral endoribonuclease vhs and  
708 cofactors to facilitate the translation of late proteins. *PLoS Pathog* *14*, e1007331.  
709 10.1371/journal.ppat.1007331.

- 710 60. Sato, Y., Kato, A., Maruzuru, Y., Oyama, M., Kozuka-Hata, H., Arii, J., and  
711 Kawaguchi, Y. (2016). Cellular Transcriptional Coactivator RanBP10 and Herpes  
712 Simplex Virus 1 ICP0 Interact and Synergistically Promote Viral Gene Expression  
713 and Replication. *J Virol* *90*, 3173-3186. 10.1128/JVI.03043-15.
- 714 61. Tanaka, M., Kagawa, H., Yamanashi, Y., Sata, T., and Kawaguchi, Y. (2003).  
715 Construction of an excisable bacterial artificial chromosome containing a full-length  
716 infectious clone of herpes simplex virus type 1: viruses reconstituted from the clone  
717 exhibit wild-type properties in vitro and in vivo. *J Virol* *77*, 1382-1391.  
718 10.1128/jvi.77.2.1382-1391.2003.
- 719 62. Merzlyak, E.M., Goedhart, J., Shcherbo, D., Bulina, M.E., Shcheglov, A.S., Fradkov,  
720 A.F., Gaintzeva, A., Lukyanov, K.A., Lukyanov, S., Gadella, T.W., and Chudakov,  
721 D.M. (2007). Bright monomeric red fluorescent protein with an extended fluorescence  
722 lifetime. *Nat Methods* *4*, 555-557. 10.1038/nmeth1062.
- 723 63. Kremers, G.J., Goedhart, J., van Munster, E.B., and Gadella, T.W., Jr. (2006). Cyan  
724 and yellow super fluorescent proteins with improved brightness, protein folding, and  
725 FRET Forster radius. *Biochemistry* *45*, 6570-6580. 10.1021/bi0516273.
- 726 64. Kato, A., Oda, S., Watanabe, M., Oyama, M., Kozuka-Hata, H., Koyanagi, N.,  
727 Maruzuru, Y., Arii, J., and Kawaguchi, Y. (2018). Roles of the Phosphorylation of  
728 Herpes Simplex Virus 1 UL51 at a Specific Site in Viral Replication and  
729 Pathogenicity. *J Virol* *92*. 10.1128/JVI.01035-18.
- 730 65. Arii, J., Takeshima, K., Maruzuru, Y., Koyanagi, N., Nakayama, Y., Kato, A., Mori,  
731 Y., and Kawaguchi, Y. (2022). Role of the Arginine Cluster in the Disordered Domain

732 of Herpes Simplex Virus 1 UL34 for the Recruitment of ESCRT-III for Viral Primary  
733 Envelopment. *J Virol* *96*, e0170421. 10.1128/JVI.01704-21.

734 66. Tischer, B.K., von Einem, J., Kaufer, B., and Osterrieder, N. (2006). Two-step red-  
735 mediated recombination for versatile high-efficiency markerless DNA manipulation  
736 in Escherichia coli. *Biotechniques* *40*, 191-197. 10.2144/000112096.

737 67. Kawaguchi, Y., Van Sant, C., and Roizman, B. (1997). Herpes simplex virus 1 alpha  
738 regulatory protein ICP0 interacts with and stabilizes the cell cycle regulator cyclin  
739 D3. *J Virol* *71*, 7328-7336. 10.1128/JVI.71.10.7328-7336.1997.

740 68. Sagou, K., Imai, T., Sagara, H., Uema, M., and Kawaguchi, Y. (2009). Regulation of  
741 the catalytic activity of herpes simplex virus 1 protein kinase Us3 by  
742 autophosphorylation and its role in pathogenesis. *J Virol* *83*, 5773-5783.  
743 10.1128/JVI.00103-09.

744 69. Ritz, C. (2010). Toward a unified approach to dose-response modeling in ecotoxicology.  
745 *Environmental Toxicology and Chemistry* *29*, 220-229. 10.1002/etc.7.

746 70. Ritz, C., Baty, F., Streibig, J.C., and Gerhard, D. (2015). Dose-Response Analysis  
747 Using R. *PLOS ONE* *10*, e0146021. 10.1371/journal.pone.0146021.  
748  
749

## ACKNOWLEDGEMENTS

We thank Risa Abe, Tohru Ikegami and Yui Muto for their excellent technical assistance.

We acknowledge the NGS core facility of the Genome Information Research Center at the Research Institute for Microbial Diseases of Osaka University for the support in RNA sequencing and data analysis.

**Funding:** This study was supported by Grants for Scientific Research and Grant-in-Aid for Scientific Research (S) (20H05692) from the Japan Society for the Promotion of Science (JSPS), grants for Scientific Research on Innovative Areas (21H00338, 21H00417, 22H04803) and a grant for Transformative Research Areas (22H05584) from the Ministry of Education, Culture, Science, Sports and Technology of Japan, PRESTO (JPMJPR22R5), SPRING (JPMJSP2018), MIRAI (JPMJMI22G1) and Moonshot R&D (JPMJM2021, JPMJMS2025) from Japan Science and Technology Agency (JST), grants (JP20wm0125002, JP22fk0108640, JP22gm1610008, JP223fa627001, JP23wm0225031, JP23wm0225035) from the Japan Agency for Medical Research and Development (AMED), grants from the International Joint Research Project of the Institute of Medical Science, the University of Tokyo, and grants from the Takeda Science Foundation, the Uehara Memorial Foundation and the Mitsubishi Foundation.

767 **Author contributions:** Conceptualization: MN, YM, YK; Methodology: MN, YM, YK;  
 768 Investigation: MN, YM, KT, FM, HK, TN, SA; Resources: MN, YM, KT, NK, AK;  
 769 Formal analysis: MN, YM, RY, TN, HP, YK, SI; Visualization: MN, YM, RY, TN, HP,  
 770 YK, SI; Funding acquisition: YM, SI, AK, YK; Writing – original draft: MN, YM, YK;  
 771 Supervision: YK

772 **Competing interests:** The authors declare that they have no competing interests.

773 **Data and materials availability:** All data needed to evaluate the conclusions in the paper  
 774 are present in the paper and/or the Supplementary Materials. The mass spectrometry data  
 775 were deposited in the Japan ProteOme STandard Repository (jPOST) under the ID  
 776 JPST002328. RNA-seq data have been deposited to Gene Expression Omnibus (GEO)  
 777 with accession number GSE240449.

778

## FIGURE LEGENDS

### **Fig. 1. Characterization of the reporter HSV-1 rICP47/vUs11 generated in this study.**

(A) Schematic diagram of the genome structure of wild-type HSV-1(F) and rICP47/vUs11. Line 1, wild-type HSV-1(F) genome; line 2, domains of the Us11 and ICP47 coding regions. The positions of insertion of TagRFP and Venus are indicated. (B) HeLa cells mock-infected or infected for 24 h with wild-type HSV-1(F) or rICP47/vUs11 at an MOI of 5 were lysed and analyzed by immunoblotting with the indicated antibodies. (C) HeLa cells were infected at an MOI of 5 with wild-type HSV-1(F) or rICP47/vUs11. Each cell culture supernatant plus the infected cells were harvested at the indicated times post infection, and progeny viruses were assayed on Vero cells. (D) HeLa cells infected for 24 h with wild-type HSV-1(F) or rICP47/vUs11 at an MOI of 5 were analyzed by flow cytometry. (E) Quantitative bar graph of the proportion of cells in the TagRFP/Venus (+/+), TagRFP/Venus (+/-), TagRFP/Venus (-/+), and TagRFP/Venus (-/-) subpopulations shown in (D). (F) CV values for TagRFP-ICP47 and Venus-Us11 shown in (D). The data are representative of three independent experiments (B and D). Each value is the mean  $\pm$  standard error of the results of four (C) or three (E and F) independent experiments. Statistical analysis was performed by unpaired Student's *t*-test. ns, not significant (C and F).

### **Fig. 2. Abundance of HSV-1 L proteins in each subpopulation of rICP47/vUs11-**

**infected cells.** (A) HeLa cells were infected for 24 h with rICP47/vUs11 at an MOI of 5 and sorted into six subpopulations (f1 to f6) by cell sorting as shown in S-Fig. 1A and

each subpopulation was analyzed by LC-MS/MS. The heatmap of  $\log_{10}$  (relative abundance) of 48 HSV-1 L proteins in each subpopulation is shown. Data are the mean values from two biologically independent experiments. (B) Heatmap of the Pearson correlation coefficient between  $\log_{10}$  (MFI of Venus) of each subpopulation and  $\log_{10}$  (relative abundance) of each HSV-1 L protein. P-values for the correlation coefficient of all HSV-1 L proteins except Us8.5 shown in (B) were  $< 0.05$ .

**Fig. 3. Quantitative analysis of a relationship between the expression levels of HSV-1 L proteins and progeny virus yields.** (A to G) HeLa cells were infected with rICP47/vUs11 at an MOI of 5 and sorted as shown in S-Fig. 2. Sorted cells were sonicated and virus titers were determined by plaque assay using Vero cells. (A) Kinetics of mean fluorescent intensity (MFI) of Venus and progeny virus titers of the entire population. (B) Scatter plot of  $\log_{10}$ (relative MFI of Venus) vs  $\log_{10}$ (PFU/ $10^4$  cells) from panel A. (C) Kinetics of progeny virus titers of the entire population from panel A (actual) and sum of the virus titers produced by f1 to f6 subpopulation (virtual\_f1-f6). The calculation method for virtual titers is described in the Materials and methods. (D) Proportion of cells in the indicated subpopulation account for the entire cell population at the indicated times after infection. (E) Proportion of virus titers produced by the f1 to f6 subpopulations account for virus titers produced by the entire population at the indicated times after infection. (F) Scatter plots of  $\log_{10}$ (relative MFI of Venus) vs  $\log_{10}$ (PFU/ $10^4$  cells). (G) Scatter plots of  $\log_{10}$ (relative MFI of Venus) vs  $\log_{10}$ (PFU/ $10^4$  cells) of the indicated subpopulations separated by time after infection from panel F. Each value is the mean  $\pm$  standard error

(A, C, D, E, F, and G) or individual value (B) of the results of three independent experiments. Statistical analysis was performed by unpaired Student's *t*-test. ns, not significant (C). Solid and dashed lines indicate 1 PFU/cell and 0.1 PFU/cell, respectively (F and G).

**Fig. 4. Cells expressing higher than specific levels of HSV-1 L proteins have a predominant role in yielding progeny infectious viruses.** (A) Kinetics of the sum of the virus titers produced by f1 to f6 (virtual\_f1-f6) or f4 to f6 (virtual\_f4-f6) subpopulations. (B) Kinetics of progeny virus titers of the entire population (actual) and sum of the virus titers produced by f4 to f6 subpopulations (virtual\_f4-f6). (C) Scatter plot of  $\log_{10}(\text{relative MFI of Venus})$  vs  $\log_{10}(\text{PFU}/10^4 \text{ cells})$  of subpopulations. (D) Progeny virus titers of the f4 to f6 subpopulations at the indicated times after infection. Each value is the mean  $\pm$  standard error (A, B and D) or individual value (C) of the results of three independent experiments. Statistical analysis was performed by unpaired Student's *t*-test. ns, not significant. All data are obtained from the experiment shown in Fig. 3.

**Fig. 5. Electron microscopic analysis of cells in the f2 to f5 subpopulations.** (A and B) HeLa cells were infected with rICP47/vUs11 at an MOI of 5 and sorted into four subpopulations (f2 to f5) by cell sorting 24 h after infection. Sorted cells were fixed, embedded, sectioned, stained, and examined by electron microscopy. (A) A transmission electron microscopy image of cells in the f2 to f5 subpopulations. n, nucleus; c, cytoplasm.

Scale bars = 500 nm. (B) The numbers of nuclear virions, enveloped virions in the perinuclear space, naked capsids in the cytoplasm, and enveloped virions in the cytoplasm of 11 cells in the f2 to f5 subpopulations were quantitated. The horizontal bars indicate the means. Virions are marked in yellow.

**Fig. 6. Frequencies of A, B, and C capsids in the nucleus of cells in the f2 to f5 subpopulations.** (A) The numbers of A, B, and C capsids in the nucleus of 11 cells analyzed in Fig. 4 in the f2 to f5 subpopulations were quantitated. The horizontal bars indicate the means. Proportions of A, B, and C capsids to nuclear capsids (B), or virions in the perinuclear space and cytoplasm (C) of cells with more than two nuclear capsids (f3, n = 9; f4, n = 11; f5, n = 11). Data are presented as the median  $\pm$  interquartile range (IQR). Statistical analysis was performed by the Mann-Whitney *U*-test, and P-values were adjusted by Bonferroni correction. ns, not significant.

**Fig. 7. Unique protein expression profiles of a subset of HSV-1 L proteins.** (A) Scatter plots of  $\log_{10}$ (relative MFI of Venus) vs  $\log_{10}$ (relative abundance) of L proteins (from S-Fig. 1B) of the bottom 10 HSV-1 L proteins with relatively low correlation coefficients between fluorescence intensity of Venus and their abundance (from Fig. 2B). Plots of terminase subunits are marked with magenta squares. (B) Threshold value (TV) of 48 L proteins (from S-Fig. 10). (C) Scatter plots of  $\log_{10}$ (relative MFI of Venus) vs  $\log_{10}$ (relative abundance) (from S-Fig. 1B) of the top 10 HSV-1 L proteins with highest TV (from S-Fig. 10). Data of terminase subunits are shown in magenta.

**Supplementary Fig. 1. Abundance of HSV-1 L proteins in each subpopulation of rICP47/vUs11 infected cells.** (A) Gating strategy for the LC-MS/MS analysis of HeLa cells infected with rICP47/vUs11 at an MOI of 5 for 24 h. (B) Scatter plots of  $\log_{10}(\text{relative MFI of Venus})$  vs  $\log_{10}(\text{relative abundances})$  of the 5 indicated HSV-1 IE proteins, 13 indicated E proteins, and 48 indicated L proteins. Each value is the mean of two biologically independent experiments. Individual value from two independent experiments is plotted as a gray circle.

**Supplementary Fig. 2. Gating strategy for the experiments shown in Fig. 3.** HeLa cells were infected with rICP47/vUs11 at an MOI of 5, analyzed by flow cytometry, and sorted into an entire cell population (FSC singlet) or f1 to f6 subpopulations by cell sorting at the indicated times after infection. Sorted cells were analyzed as shown in Fig 3.

**Supplementary Fig. 3. Quantitative analysis of the relationship between the expression levels of HSV-1 L proteins and progeny virus yields at different MOIs.** (A to G) HeLa cells infected with rICP47/vUs11 at the indicated MOI for 24 h, were sorted into f1 to f6 subpopulations (A), sonicated and virus titers were determined by plaque assay using Vero cells. (B) Scatter plot of  $\log_{10}(\text{relative MFI of Venus})$  vs  $\log_{10}(\text{PFU}/10^4 \text{ cells})$ . (C) Proportion of cells in the indicated subpopulations account for the entire cell population at the indicated MOIs. (D) Proportion of virus titers produced by the f1 to f6 subpopulations account for virus titers produced by the entire population

at the indicated times after infection. (E to G) Progeny virus titers of the entire population (actual) and sum of the virus titers produced by f1 to f6 (virtual\_f1-f6) or f4 to f6 (virtual\_f4-f6) subpopulations at the indicated MOIs. The data are representative of five independent experiments (A). Each value is the mean  $\pm$  standard error of the results of five independent experiments (B to G). Statistical analysis was performed by one-way ANOVA followed by the Tukey test (E to G). n.s., not significant

**Supplementary Fig. 4. Quantitative analysis of the relationship between the expression levels of HSV-1 L proteins and progeny virus yields using different cell lines.** Vero (A to E), U2OS (F to J), HaCaT (K to O), or HFFF-2 (P to T) cells infected with rICP47/vUs11 at an MOI of 1 (A to E, and K to T) or 2.5 (F to J) for 12 h, were sorted into f1 to f6 subpopulations (A, F, K, and P), sonicated, and virus titers were determined by plaque assay using Vero cells. (B, G, L, and Q) Scatter plots of  $\log_{10}(\text{relative MFI of Venus})$  vs  $\log_{10}(\text{PFU}/10^4 \text{ cells})$  of each subpopulation. (C, H, M, and R) Proportion of cells in the f1 to f6 subpopulations account for the entire cell population. (D, I, N, and S) Proportion of virus titers produced by each subpopulation account for the virus titers produced by the entire cell population. (E, J, O, and T) Progeny virus titers of the entire population (actual) and sum of the virus titers produced by f1 to f6 or f4 to f6 subpopulations. The data are representative of three (F) or four (A, K, and P) independent experiments. Each value is the mean  $\pm$  standard error of the results of three (G to J) or four (B to E, L to O, and Q to T) independent experiments. Solid and dashed lines indicate 1 PFU/cell and 0.1 PFU/cell, respectively (B, G, L and Q). Statistical

analysis was performed by one-way ANOVA followed by the Tukey test. n.s., not significant (E, J, O, and T).

**Supplementary Fig. 5. Electron microscopic analysis of cells in the f2 to f4 subpopulations at 8 h after infection.** (A and B) HeLa cells were infected with rICP47/vUs11 at an MOI of 5 and sorted into three subpopulations (f2 to f4) by cell sorting 8 h after infection. Sorted cells were fixed, embedded, sectioned, stained, and examined by electron microscopy. (A) A transmission electron microscopy image of cells in the f2 to f4 subpopulations. n, nucleus; c, cytoplasm. Scale bar = 500 nm. (B) The numbers of nuclear virions, enveloped virions in the perinuclear space, naked capsids in the cytoplasm, and enveloped virions in the cytoplasm of 11 cells in the f2 to f4 subpopulations were quantitated. The horizontal bars indicate the means. Enveloped virions and naked capsids are marked in yellow.

**Supplementary Fig. 6. f4 to f6 subpopulations have a predominant role in yielding progeny infectious viruses.** (A) Scatter plots of  $\log_{10}(\text{relative MFI of Venus})$  vs PFU/ $10^4$  cells of the indicated subpopulation separated by time after infection from Fig. 3 panel G. Scatter plots under the same conditions of electron microscopic analysis performed in Fig. 5 and S-Fig. 5 are shown in magenta. (B) Progeny virus titers of the f4 to f6 subpopulations at the indicated times after infection from Fig. 4 panel B. Statistical analysis was performed by one-way ANOVA followed by the Tukey test. n.s., not significant.

933

934 **Supplementary Fig. 7. Amount of HSV-1 DNA and mRNA in the f1 to f6**  
 935 **subpopulations.** (A and B) HeLa cells were infected for 24 h with rICP47/vUs11 at an  
 936 MOI of 5 and sorted into six subpopulations (f1 to f6) by cell sorting. Relative amounts  
 937 of HSV-1 DNA (A) and mRNA (B) of selected genes in each subpopulation were  
 938 analyzed by quantitative PCR or RNA-seq, respectively. Scatter plot of  $\log_{10}(\text{relative MFI}$   
 939  $\text{of Venus})$  vs  $\log_{10}(\text{relative amount of HSV-1 DNA})$  (A), or scatter plots of  $\log_{10}(\text{relative}$   
 940  $\text{MFI of Venus})$  vs  $\log_{10}(\text{relative FPKM})$  of the indicated HSV-1 genes (B) are shown.  
 941 Each value is the mean  $\pm$  standard error of the results of three biologically independent  
 942 samples.

943

944 **Supplementary Fig. 8. Frequency of A, B, and C capsids in the nucleus of cells in f2**  
 945 **to f5 subpopulations.** A transmission electron microscopy image of cells in the f2 to f5  
 946 subpopulations. n, nucleus; c, cytoplasm from the experiment in Fig. 6. Type A capsids  
 947 are marked in green, B capsids in blue, and C capsids in red. Scale bars = 500 nm.

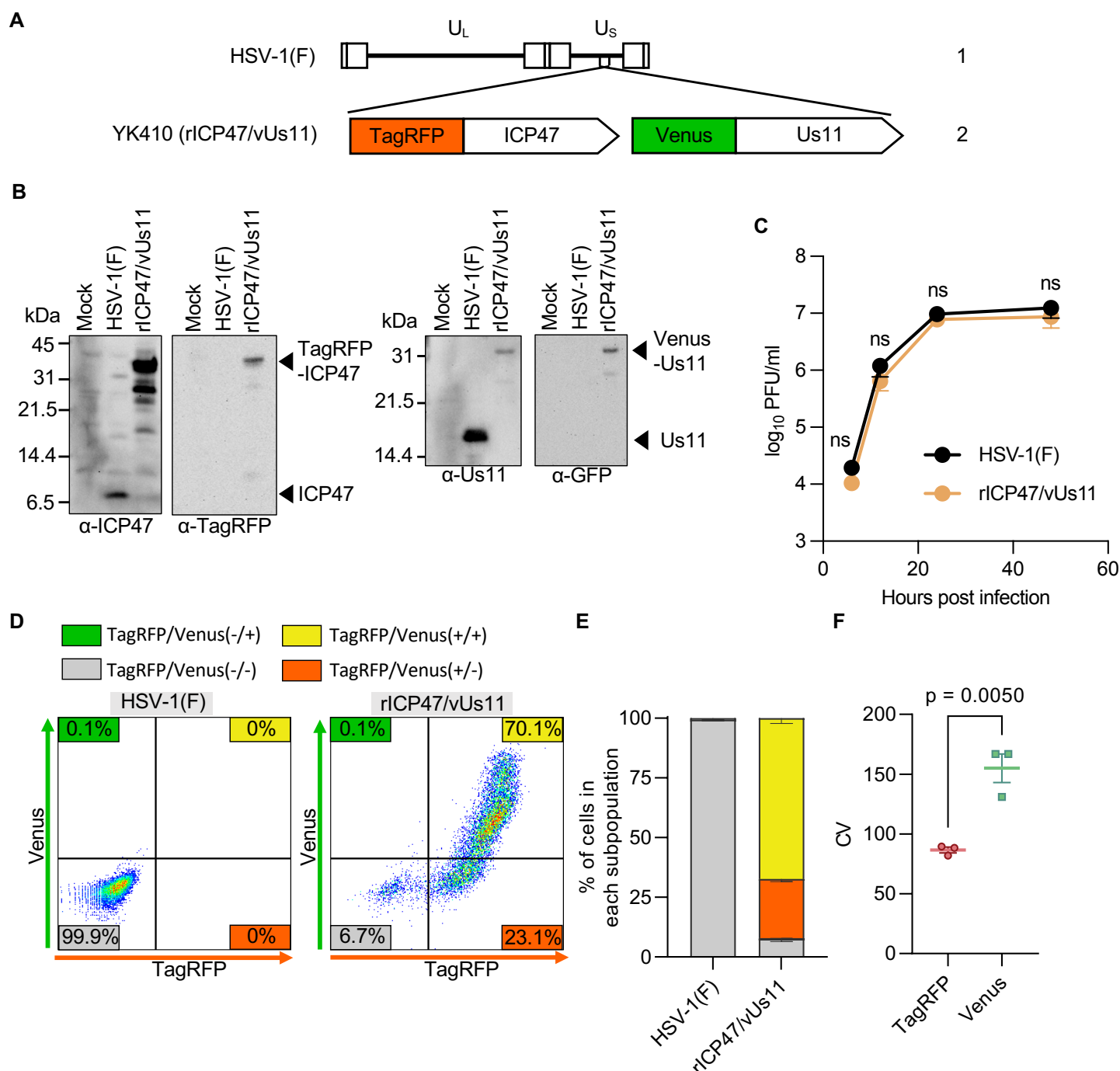
948

949 **Supplementary Fig. 9. Frequencies of B and C capsids in the nucleus of cells in the**  
 950 **f2 to f4 subpopulations at 8 h after infection.** (A) A transmission electron microscopy  
 951 image of cells in the f2 to f4 subpopulations. n, nucleus; c, cytoplasm from the experiment  
 952 in S-Fig. 6. Type A capsids are marked in green, B capsids in blue, and C capsids in red.  
 953 Scale bar = 500 nm. (B) The numbers of A, B, and C capsids in the nucleus of 11 cells  
 954 analyzed in S-Fig. 6 in the f2 to f4 subpopulations were quantitated. The horizontal bars

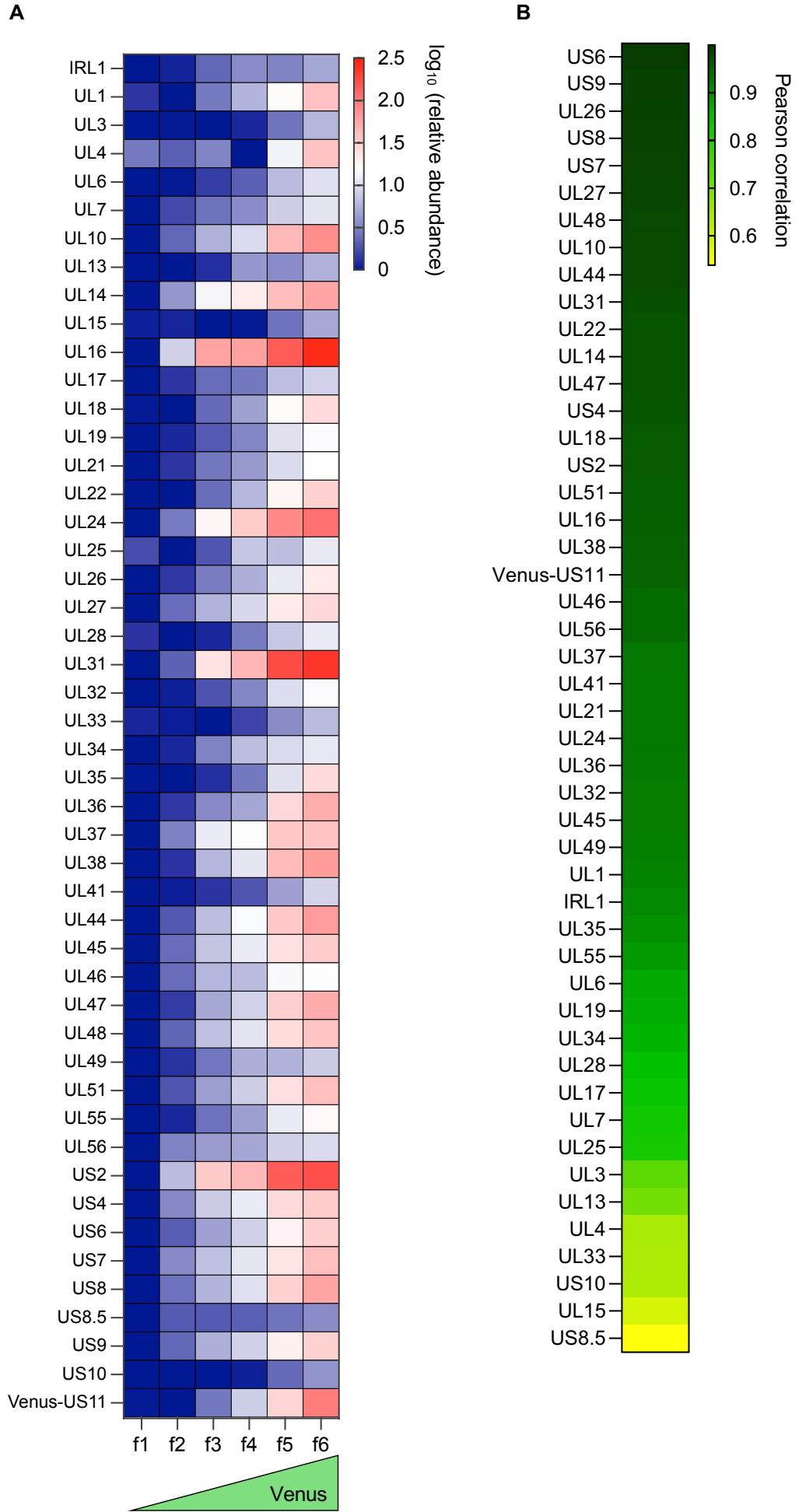
indicate the means. Proportions of B and C capsids to nuclear capsids (C), or virions in the perinuclear space and cytoplasm (D) of cells with more than two nuclear capsids (f3, n = 11; f4, n = 11). Data are presented as the median  $\pm$  interquartile range (IQR). Statistical analysis was performed by the Mann-Whitney *U*-test.

**Supplementary Fig. 10. Curve fitting to abundance profiles of HSV-1 L proteins.**

Scatter plots of  $\log_{10}$ (relative MFI of Venus) vs  $\log_{10}$ (relative abundances) of the 48 indicated HSV-1 L proteins (from S-Fig. 1B) were fitted to a four-parameter logistic regression curve. TVs are the x-axis value at which the y-axis value increases by  $\log_{10}2$  (2-fold increase in linear scale) from the starting point ( $x = 0$ ) for each curve. The grey regions correspond to 95% confidence intervals. The average value of two biologically independent experiments was used for curve fitting.



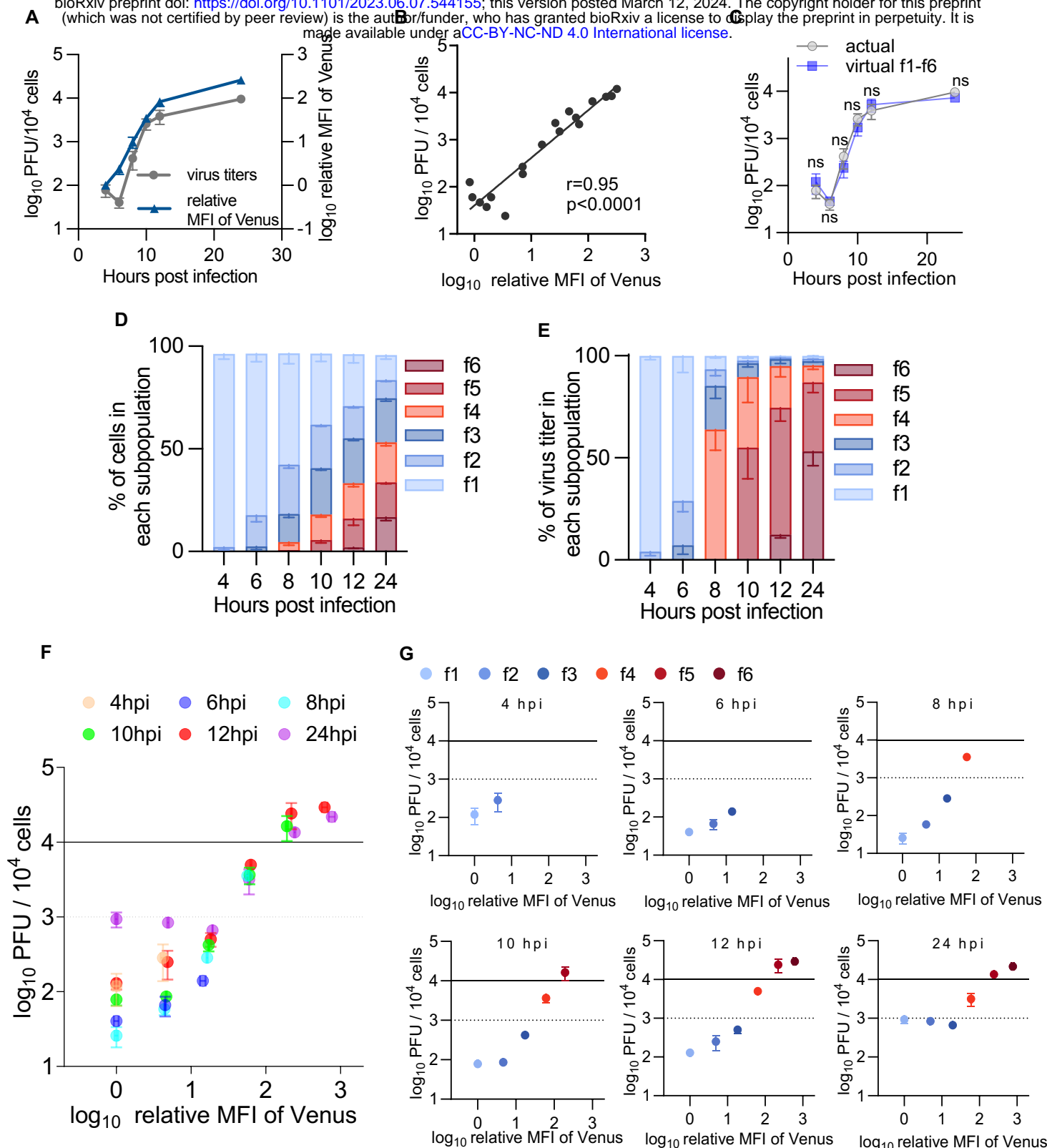
**Fig. 1. Characterization of the reporter HSV-1 rICP47/vUs11 generated in this study.** (A) Schematic diagram of the genome structure of wild-type HSV-1(F) and rICP47/vUs11. Line 1, wild-type HSV-1(F) genome; line 2, domains of the Us11 and ICP47 coding regions. The positions of insertion of TagRFP and Venus are indicated. (B) HeLa cells mock-infected or infected for 24 h with wild-type HSV-1(F) or rICP47/vUs11 at an MOI of 5 were lysed and analyzed by immunoblotting with the indicated antibodies. (C) HeLa cells were infected at an MOI of 5 with wild-type HSV-1(F) or rICP47/vUs11. Each cell culture supernatant plus the infected cells were harvested at the indicated times post infection, and progeny viruses were assayed on Vero cells. (D) HeLa cells infected for 24 h with wild-type HSV-1(F) or rICP47/vUs11 at an MOI of 5 were analyzed by flow cytometry. (E) Quantitative bar graph of the proportion of cells in the TagRFP/Venus (+/+), TagRFP/Venus (+/-), TagRFP/Venus (-/+), and TagRFP/Venus (-/-) subpopulations shown in (D). (F) CV values for TagRFP-ICP47 and Venus-Us11 shown in (D). The data are representative of three independent experiments (B and D). Each value is the mean  $\pm$  standard error of the results of four (C) or three (E and F) independent experiments. Statistical analysis was performed by unpaired Student's *t*-test. ns, not significant (C and F).



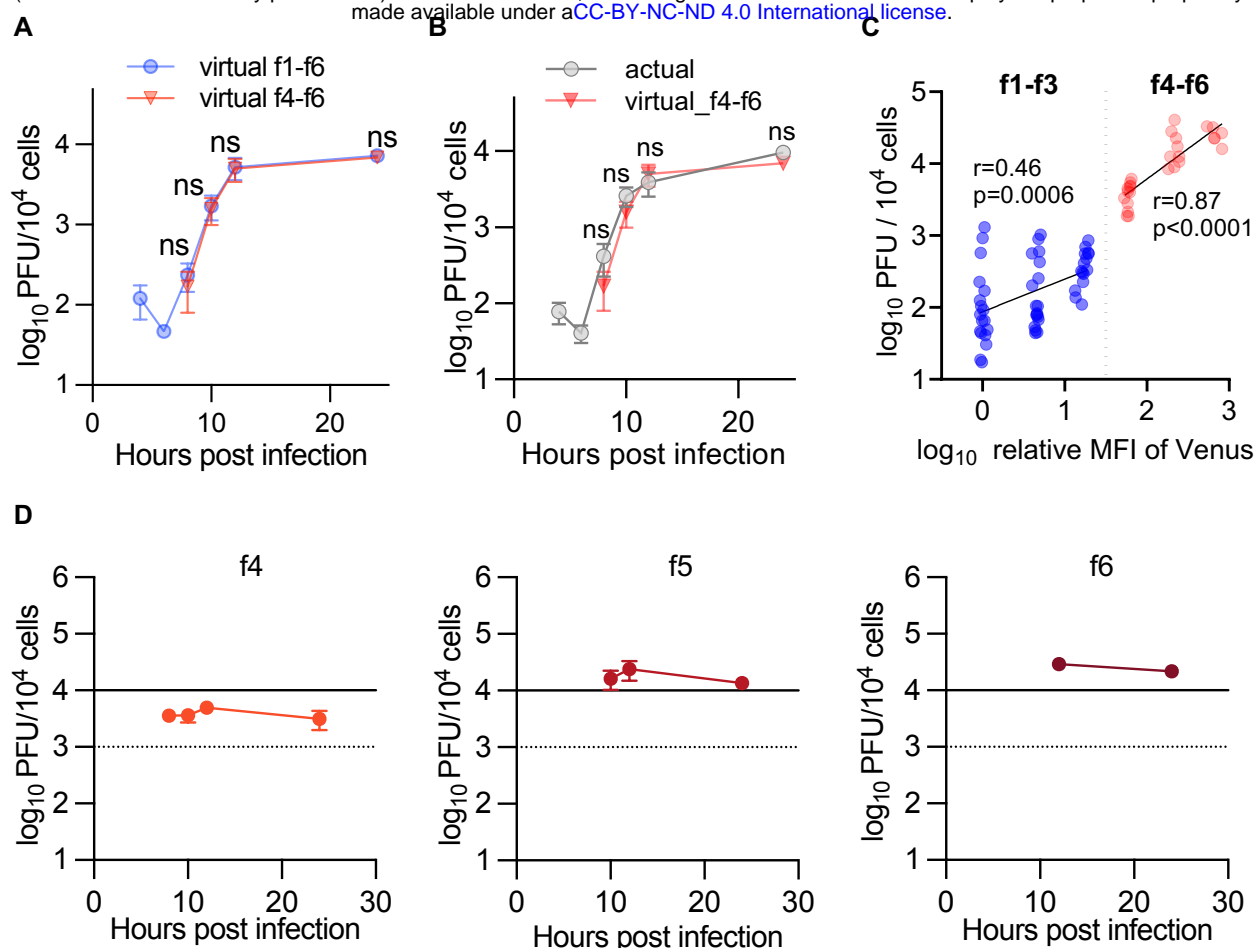
(Legend on next page)

Fig. 2 M. Nobe and Y. Maruzuru et al.

**Fig. 2. Abundance of HSV-1 L proteins in each subpopulation of rICP47/vUs11-infected cells.** (A) HeLa cells were infected for 24 h with rICP47/vUs11 at an MOI of 5 and sorted into six subpopulations (f1 to f6) by cell sorting as shown in S-Fig. 1A and each subpopulation was analyzed by LC-MS/MS. The heatmap of log<sub>10</sub> (relative abundance) of 48 HSV-1 L proteins in each subpopulation is shown. Data are the mean values from two biologically independent experiments. (B) Heatmap of the Pearson correlation coefficient between log<sub>10</sub> (MFI of Venus) of each subpopulation and log<sub>10</sub> (relative abundance) of each HSV-1 L protein. P-values for the correlation coefficient of all HSV-1 L proteins except Us8.5 shown in (B) were < 0.05.

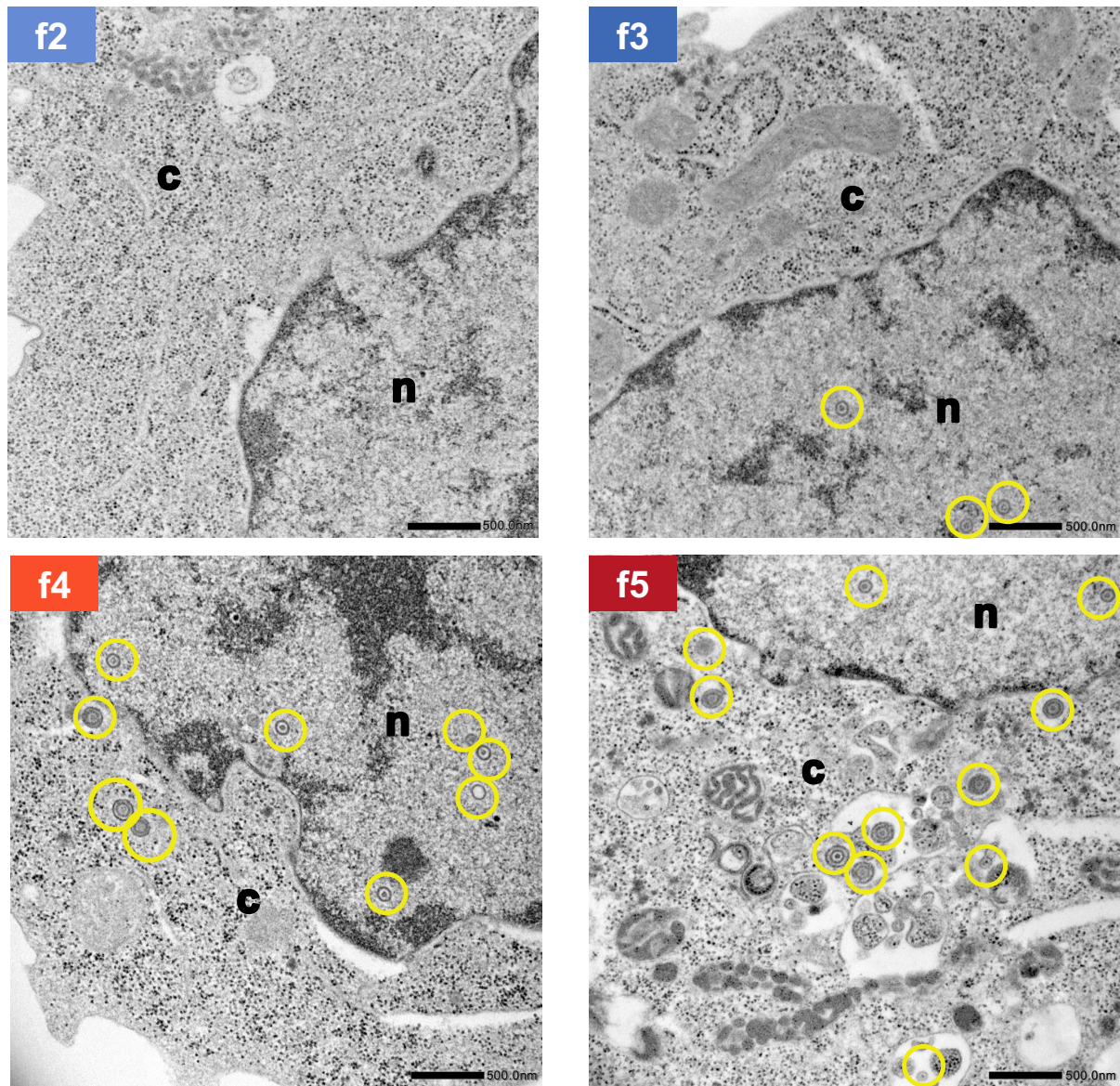


**Fig. 3. Quantitative analysis of a relationship between the expression levels of HSV-1 L proteins and progeny virus yields.** (A to G) HeLa cells were infected with rICP47/vUs11 at an MOI of 5 and sorted as shown in S-Fig. 2. Sorted cells were sonicated and virus titers were determined by plaque assay using Vero cells. (A) Kinetics of mean fluorescent intensity (MFI) of Venus and progeny virus titers of the entire population. (B) Scatter plot of  $\log_{10}$ (relative MFI of Venus) vs  $\log_{10}$ (PFU/ $10^4$  cells) from panel A. (C) Kinetics of progeny virus titers of the entire population from panel A (actual) and sum of the virus titers produced by f1 to f6 subpopulation (virtual\_f1-f6). The calculation method for virtual titers is described in the Materials and methods. (D) Proportion of cells in the indicated subpopulation account for the entire cell population at the indicated times after infection. (E) Proportion of virus titers produced by the f1 to f6 subpopulations account for virus titers produced by the entire population at the indicated times after infection. (F) Scatter plots of  $\log_{10}$ (relative MFI of Venus) vs  $\log_{10}$ (PFU/ $10^4$  cells). (G) Scatter plots of  $\log_{10}$ (relative MFI of Venus) vs  $\log_{10}$ (PFU/ $10^4$  cells) of the indicated subpopulations separated by time after infection from panel F. Each value is the mean  $\pm$  standard error (A, C, D, E, F, and G) or individual value (B) of the results of three independent experiments. Statistical analysis was performed by unpaired Student's *t*-test. ns, not significant (C). Solid and dashed lines indicate 1 PFU/cell and 0.1 PFU/cell, respectively (F and G).



**Fig. 4. Cells expressing higher than specific levels of HSV-1 L proteins have a predominant role in yielding progeny infectious viruses.** (A) Kinetics of the sum of the virus titers produced by f1 to f6 (virtual\_f1-f6) or f4 to f6 (virtual\_f4-f6) subpopulations. (B) Kinetics of progeny virus titers of the entire population (actual) and sum of the virus titers produced by f4 to f6 subpopulations (virtual\_f4-f6). (C) Scatter plot of  $\log_{10}$ (relative MFI of Venus) vs  $\log_{10}$ (PFU/ $10^4$  cells) of subpopulations. (D) Progeny virus titers of the f4 to f6 subpopulations at the indicated times after infection. Each value is the mean  $\pm$  standard error (A, B and D) or individual value (C) of the results of three independent experiments. Statistical analysis was performed by unpaired Student's *t*-test. ns, not significant. All data are obtained from the experiment shown in Fig. 3.

A



B

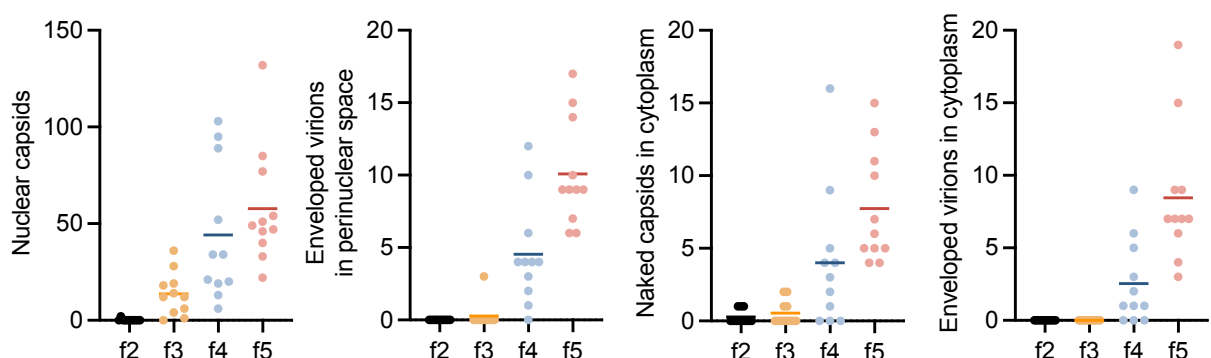


**Fig. 5. Electron microscopic analysis of cells in the f2 to f5 subpopulations.** (A and B) HeLa cells were infected with rICP47/vUs11 at an MOI of 5 and sorted into four subpopulations (f2 to f5) by cell sorting 24 h after infection. Sorted cells were fixed, embedded, sectioned, stained, and examined by electron microscopy. (A) A transmission electron microscopy image of cells in the f2 to f5 subpopulations. n, nucleus; c, cytoplasm. Scale bars = 500 nm. (B) The numbers of nuclear virions, enveloped virions in the perinuclear space, naked capsids in the cytoplasm, and enveloped virions in the cytoplasm of 11 cells in the f2 to f5 subpopulations were quantitated. The horizontal bars indicate the means. Virions are marked in yellow.

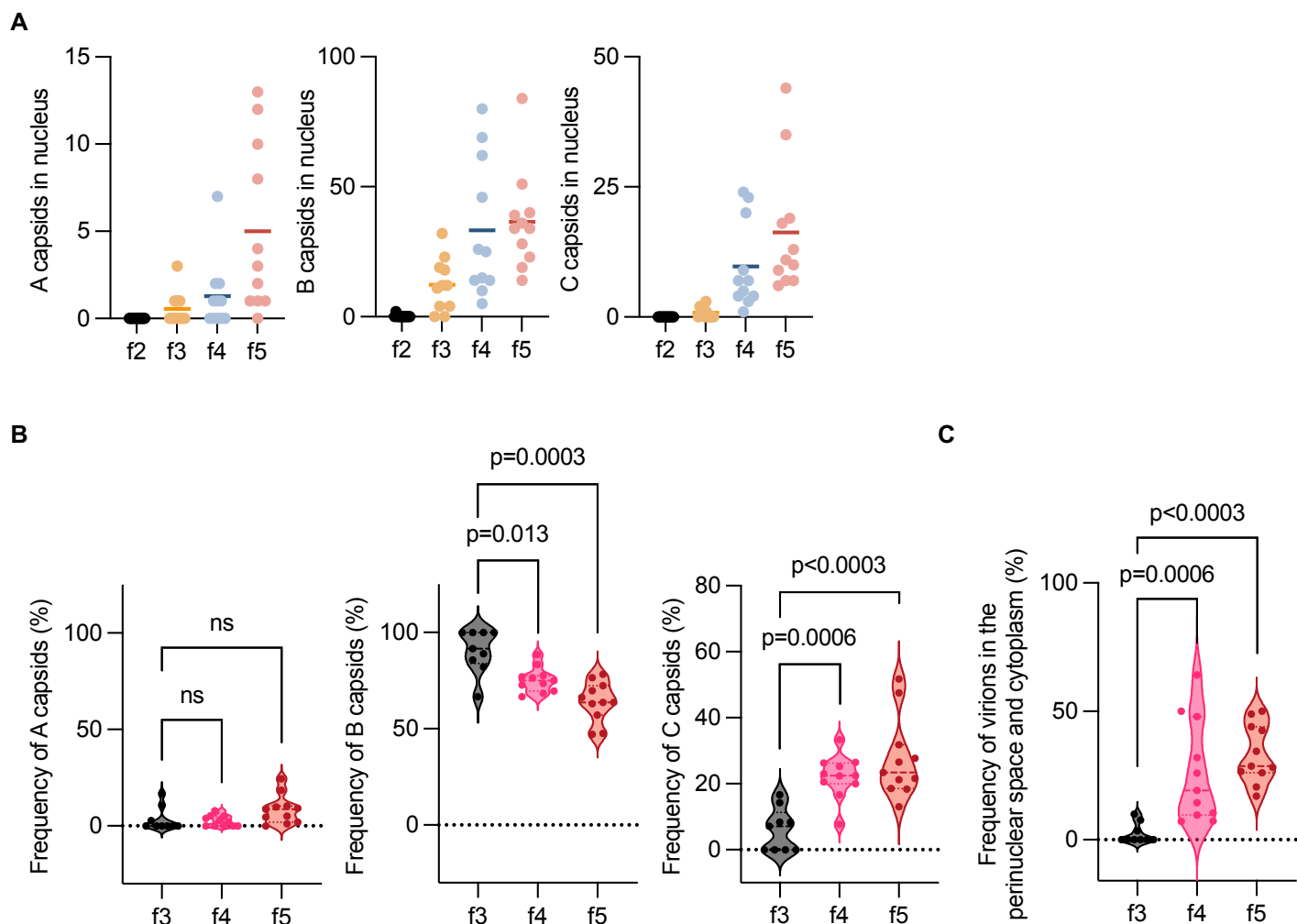


**Fig. 6. Frequencies of A, B, and C capsids in the nucleus of cells in the f2 to f5 subpopulations.** (A) The numbers of A, B, and C capsids in the nucleus of 11 cells analyzed in Fig. 4 in the f2 to f5 subpopulations were quantitated. The horizontal bars indicate the means. Proportions of A, B, and C capsids to nuclear capsids (B), or virions in the perinuclear space and cytoplasm (C) of cells with more than two nuclear capsids (f3, n = 9; f4, n = 11; f5, n = 11). Data are presented as the median  $\pm$  interquartile range (IQR). Statistical analysis was performed by the Mann-Whitney *U*-test, and P-values were adjusted by Bonferroni correction. ns, not significant.

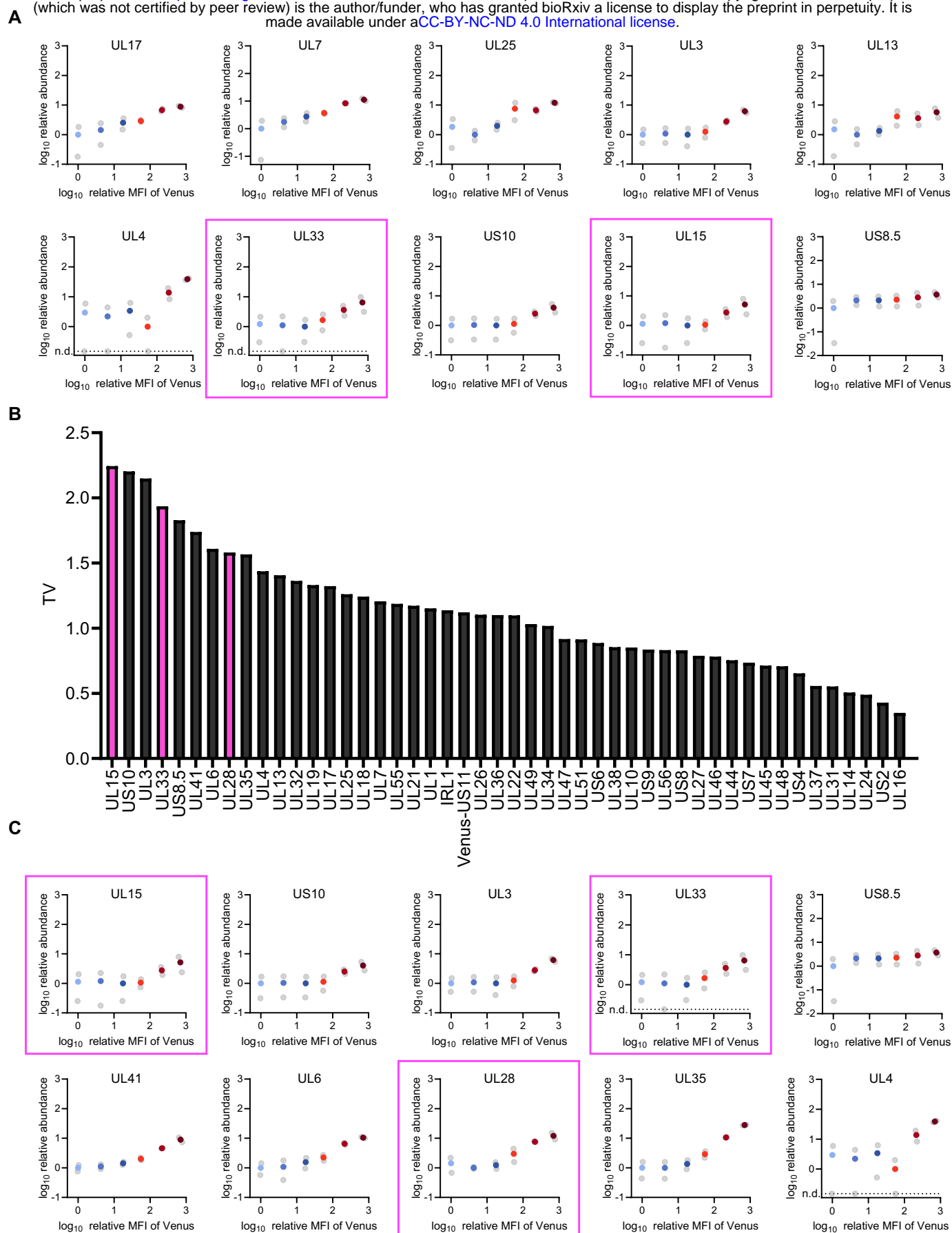


**Fig. 7. Unique protein expression profiles of a subset of HSV-1 L proteins.** (A) Scatter plots of  $\log_{10}(\text{relative MFI of Venus})$  vs  $\log_{10}(\text{relative abundance})$  of L proteins (from S-Fig. 1B) of the bottom 10 HSV-1 L proteins with relatively low correlation coefficients between fluorescence intensity of Venus and their abundance (from Fig. 2B). Plots of terminase subunits are marked with magenta squares. (B) Threshold value (TV) of 48 L proteins (from S-Fig. 10). (C) Scatter plots of  $\log_{10}(\text{relative MFI of Venus})$  vs  $\log_{10}(\text{relative abundance})$  (from S-Fig. 1B) of the top 10 HSV-1 L proteins with highest TV (from S-Fig. 10). Data of terminase subunits are shown in magenta.